Remote Sensing of Environment 323 (2025) 114721

Contents lists available at ScienceDirect

Remote Sensing of Environment

journal homepage: www.elsevier.com/locate/rse

Spatially continuous mapping of pre-fire fuel characteristics with imaging spectroscopy and lidar for fire emissions modeling

Clare M. Saiki [a,*], Dar A. Roberts [a], E. Natasha Stavros [b], Andrew T. Hudak [c], Nancy H.F. French [d], Olga Kalashnikova [e], Michael J. Garay [f], T. Ryan McCarley [g], Mark Corrao [h,i]

[a] University of California Santa Barbara, Department of Geography, Santa Barbara, CA 93106, USA
[b] WKID Solutions, Boulder, CO 80303, USA
[c] U.S. Department of Agriculture Forest Service, Rocky Mountain Research Station, Moscow, ID 83843, USA
[d] Michigan Tech Research Institute, Michigan Technological University, Ann Arbor, MI 48105, USA
[e] NASA Jet Propulsion Laboratory, California Institute of Technology, Pasadena, CA 91109, USA
[f] Aerospace Corporation, Pasadena, CA 91101, USA
[g] University of Idaho, College of Natural Resources, Moscow, ID 83844, USA
[h] University of Idaho, Department of Forest, Rangeland, and Fire Sciences, College of Natural Resources, Moscow, ID 83844, USA
[i] Northwest Management Incorporated, Moscow, ID 83843, USA

ARTICLE INFO

Editor Name: Dr. Marie Weiss

Keywords:
Fuels
Imaging spectroscopy
LiDAR
Fire emissions
Fire effects
Vegetation models

ABSTRACT

Fuels are a large source of uncertainty in fire emissions estimates due to variability in the physical and chemical properties of fuels and how they are represented. These uncertainties can be addressed using imaging spectroscopy and lidar data, that provide observations of the chemical and physical traits and spatial distribution of vegetation. Combined with ground fuel measurements, these data provide information on fuel distribution and quantity important for mapping and modeling fire effects. In this study, we present a methodology to develop models and continuous maps of pre-fire fuel characteristics for use in fire emissions modeling. We first addressed any spatial gaps over fire areas for Airborne Visible/Infrared Imaging Spectrometer (AVIRIS) chemical trait data using Random Forests regression and for derived fractional cover. We used the AVIRIS fractional cover and chemical traits or AVIRIS estimates alongside lidar, multispectral, and topographic variables to build fuel characteristic models informed by ground measurements with partial least squares regression. We derived maps of predictive uncertainty alongside a suite of uncertainty statistics for each fuel characteristic that inform the use of fuels data within fire effects models. We used two study sites: the Williams Flats wildfire in eastern Washington state, USA and three prescribed crown fires in Utah, USA. The results show similar error between calibration and validation sets and NRMSE of around 20 % or lower for a majority of the fuel models. We present fuel characteristic and uncertainty maps for all fires. This study shows that the use of imaging spectroscopy and lidar data have the potential to represent fuel heterogeneity and continuously map fuel characteristics for fire effects modeling.

1. Introduction and background

The frequency, severity, and extent of wildfires are projected to increase in the western United States due to rising temperatures attributed to climate change (Stephens et al., 2013; Stavros et al., 2014). The quantity of area burned by wildfires has approximately quadrupled in the United States in the past forty years (Burke et al., 2021), and fire climatology studies suggest that in the coming decades, the annual area burned will continue to increase (McKenzie et al., 2004; Flannigan et al., 2009; Littell et al., 2010; Liu and Goodrick, 2013; McKenzie et al., 2014). Climate change impacts that lead to an increased incidence of large wildfires are already apparent in the American Southwest (Dennison et al., 2014).

Globally, wildfires are a significant source of greenhouse gasses and aerosol emissions (Seiler and Crutzen, 1980) that impact climate, air quality (Wegesser et al., 2009; Larkin et al., 2010), and human health

* Corresponding author.
E-mail address: claresaiki@ucsb.edu (C.M. Saiki).

https://doi.org/10.1016/j.rse.2025.114721
Received 22 October 2024; Received in revised form 19 March 2025; Accepted 21 March 2025
Available online 29 March 2025

(US EPA, 2019). Wildfire smoke is a complex mixture of particle pollutants that have a variety of adverse health effects, such as increased susceptibility to respiratory diseases and increased risk of heart attack or failure (US EPA, 2020). Because wildfires are projected to increase in frequency, severity, and extent, so too will the effects of fire emissions on climate and human populations. The source of wildfire emissions are fire fuels, the vegetation and biomass that burns in a fire. Fire fuels combined with heat, intensity, and residence time of fire influence the emissions from fire. Fire fuels (henceforth simplified to fuels) are inherently continuous (Keane, 2015) and contribute to a large portion of the uncertainty in fire emissions estimates due to errors in the representations of fuel properties and their variability (French et al., 2004; Ottmar, 2014; Prichard et al., 2019; Kennedy et al., 2020; Fortin, 2021). Fuels influence the type of combustion that occurs and subsequently the chemical composition of smoke (Urbanski et al., 2011; McKenzie et al., 2014). The composition of fire emissions is influenced by the properties and characteristics of fuels alongside fire behavior (Christian et al., 2003).

The common approach to modeling wildfire emissions uses static, categorically homogenous fuels information. These homogenous fuel representations do not capture seasonal changes and over-simplify the heterogeneity of fuel type, structure, and distribution (Stavros et al., 2018). Fire emissions estimates are reliant upon fuel consumption and fuels information like physical characteristics (e.g. height, cover, fuel loading, bulk density, etc.) and condition (e.g. moisture). Fire effects models, such as CONSUME (Prichard, 2007), Global Fire Emissions Database (GFED; Randerson et al., 2018), and CANFIRE (de Groot, 2012) integrate fuels information—including physical characteristics—and meteorological conditions to estimate fuel loads, consumption, and subsequently derive emissions using emission factors. Some studies have found as much as 80 % of the error in calculating source emissions may be attributed to errors in estimating fuel characteristics (Peterson, 1987; Larkin et al., 2012). In consumption and emissions models, fuels are often defined as a set of fuel properties associated with a categorical fuel type or fuelbed. These are further defined by dominant vegetation type (e.g., conifer forest, shrubland), fuel stratum (e.g. tree crown, understory shrubs, surface material or duff), and management/disturbance history (Ottmar et al., 2007). Fuels are often represented this way because of existing methods for categorical remotely sensed fuel estimates, low spatial and temporal data resolution, and low accuracy (Andreu et al., 2012; Gale et al., 2021; Parresol et al., 2012).

Because direct measurement and observation of fuel characteristics and properties are limited on the ground, remote sensing has played an important role in defining fuel classifications, often in combination with ancillary information such as insolation, slope, or aspect (Chuvieco and Salas, 1996) or predictive landscape modeling (e.g., LANDFIRE; Rollins, 2009; Ryan and Opperman, 2013). Operationally used fuels datasets, like LANDFIRE, incorporate remote sensing data but requires expert knowledge to assign appropriate fuel classifications. Additionally, these data products may need adjustments to ensure appropriate application at local scales (Rollins, 2009). Many studies have produced fuel model and fuel type classification maps using a variety of multispectral imagery, lidar, and ancillary data (e.g. Mutlu et al., 2008; Marino et al., 2016; García et al., 2017; Domingo et al., 2020). While these maps capture spatial patterns, they often rely on generalized, discrete fuel classifications or conceptual relationships that do not directly link fuels to fire effects (Gale et al., 2021). Through the use of remotely measured fuel characteristics rather than classifications, it is possible to move away from standard and subjective (Keane et al., 2001) homogenous representations of fuels that contribute to error in estimating emissions (Stavros et al., 2018).

Remote sensing, specifically imaging spectroscopy, allows for improved representations of fuel characteristics due to detailed spectral data that detect small variations in spectral reflectance between fuel types (Roberts et al., 2006; Lasaponara et al., 2006; Veraverbeke et al., 2018). Imaging spectroscopy data can advance our ability to map fuel characteristics through direct, continuous, and variable estimates of key vegetation traits and biochemical properties that replace coarse and uniform representations of fuels. Due to known wavelength associated biochemical absorption features (Curran, 1989; Curran et al., 1992; Fourty et al., 1996; Curran et al., 2001), vegetation traits that influence processes that are related to photosynthesis and primary productivity, nutrient cycling, and even litter decomposition, can be mapped with imaging spectroscopy (Evans, 1989; Reich et al., 1997; Wright et al., 2004; Cornwell et al., 2008). These vegetation traits and biochemical properties include canopy moisture (Serrano et al., 2000), leaf mass (Leaf Area Index; LAI, Roberts et al., 2004, Leaf Mass per Area: LMA, Singh et al., 2015), and foliar functional traits like canopy nitrogen content (Martin et al., 2008), lignin, and carbon. Imaging spectroscopy data can additionally be used to quantify vegetation condition through estimates of fractional cover of green or photosynthetic vegetation, non-photosynthetic vegetation, substrate, and ash and char on a sub-pixel level (Roberts et al., 1998).

Similarly, continuous structural attributes, such as canopy bulk density, crown base height, and crown volume can be mapped at a fine scale using Light Detection and Ranging (lidar: Falkowski et al., 2006, 2009; Wulder et al., 2012; Hudak et al., 2020; Mauro et al., 2021). Airborne imaging spectroscopy and lidar sensors provide complementary fuels information and are mature remote sensing technologies that have consistently demonstrated utility for observations of vegetation and ecosystem functioning (NRC Decadal Survey, 2018; Gale et al., 2021). Together with fire emissions models, these remote sensing techniques offer the potential to improve our ability to quantify fuel characteristics and their spatial variability that can reduce uncertainty in fire emissions estimates.

Methods to continuously quantify fuel characteristics for fire effects modeling and estimates using hyperspectral data have not been fully explored; especially methods that capture spatial and temporal variability appropriately (Stavros et al., 2018). Accurate estimates of fire emissions are critical to assess air quality, continental and global carbon fluxes, and the influence of fire on climate. Better representations of pre-fire fuels are the first step.

Our objective is to evaluate the potential for using imaging spectroscopy and lidar data to model, continuously map, and quantify uncertainty of pre-fire fuel characteristics that can be used for fire consumption and emissions modeling. We develop physical fuel characteristic models at multiple study sites for a wildfire and prescribed (Rx) crown fires studied for smoke emissions, apply the models to continuously map fuel characteristics where a fire burns, and evaluate and quantify uncertainty through the modeling and mapping process.

2. Materials and methods

2.1. Study sites

A large wildfire in eastern Washington state and three stand-replacing prescribed crown fires in southern Utah were used in this study characterizing fuels for estimating fire emissions (Fig. 1). Fire emissions can be estimated from both wildfires and Rx fires, so this study includes both classes of wildland fires that met the objectives of two large fire campaigns: the Fire Influence on Regional to global Environments and Air Quality (FIREX-AQ) campaign jointly led by NASA and NOAA, and the Fire and Smoke Model Evaluation Experiment (FASMEE) led by the U.S. Forest Service. Both campaigns prioritized data collections on these fires in large part because there was existing (e.g., pre-fire) lidar available for the characterization of pre-fire vegetation and fuels that could complement the suite of data collected by the collaborating campaigns. Airborne and field data describing fuels were collected through FIREX-AQ and FASMEE and used in this study.

2.1.1. Williams Flats fire

The 17,987 ha Williams Flats (WF) wildfire was ignited by lightning

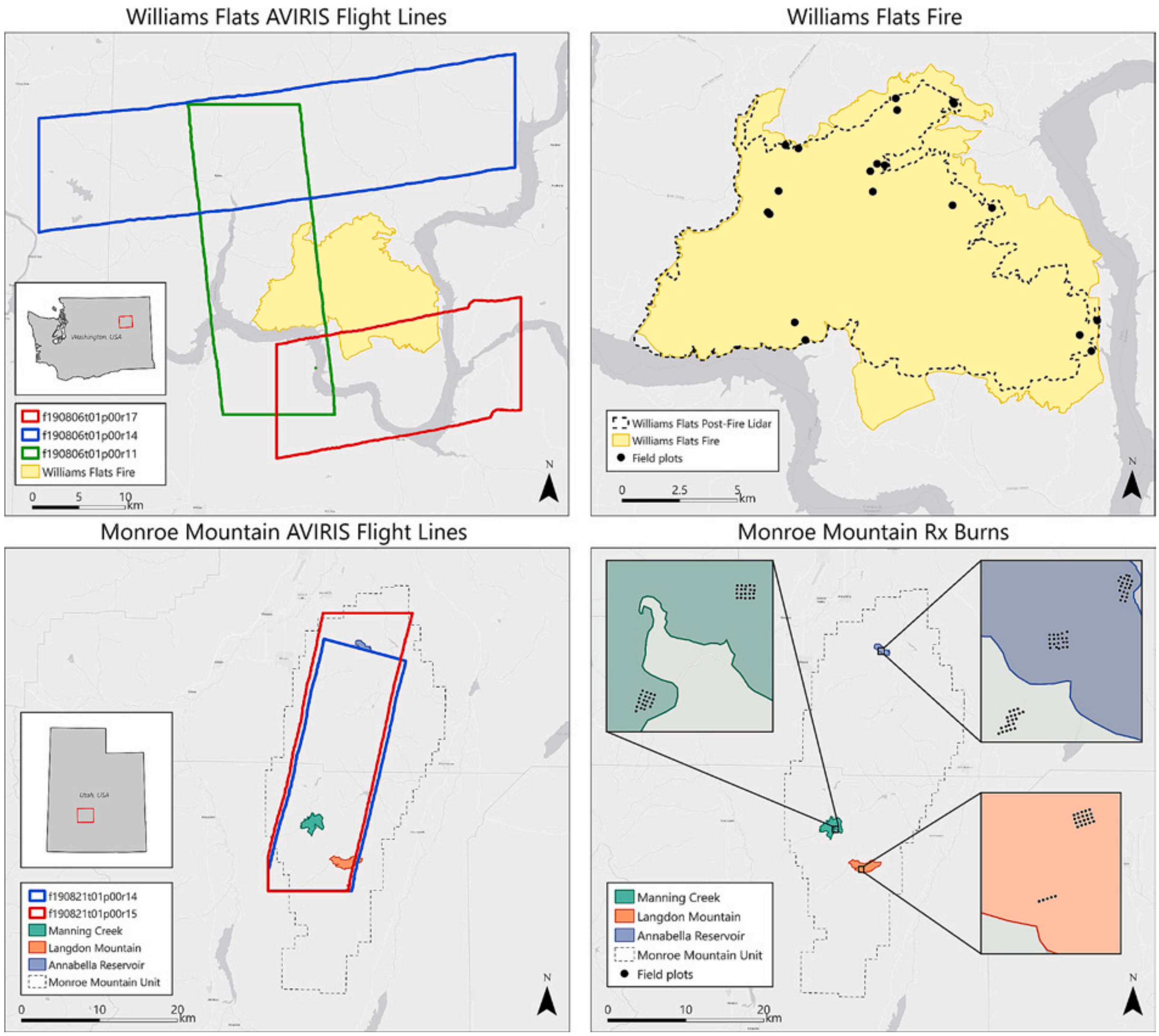

Fig. 1. Locations of a wildfire in Washington, USA and three prescribed (Rx) burns on Monroe Mountain in Fishlake National Forest in Utah, USA. The AVIRIS flightline coverage is shown on the maps on the left, and the lidar coverage extent and field sample plot locations are shown on the right.

on 2 August 2019 on land of the Confederated Colville Tribe near Keller Washington (Fig. 1). FIREX-AQ collected hyperspectral imagery of the active fire areas on 6–8 August 2019 from an ER-2 aircraft at high altitude. FASMEE collected tree, vegetation, and fuel measurements in 20 field plots in September 2019, the month after the wildfire, across burn severity conditions ranging from unburned to high severity and vegetation ranging from sagebrush scrub to ponderosa pine forest and mixed conifer forest. Because this was a wildfire, all field plots were installed post-fire based on a stratified random design to sample across the major vegetation types (as indicated by LANDFIRE Existing Vegetation Types) and burn severity classes (High, Moderate, Low, and Unburned as indicated by classified dNBR) across the post-fire landscape, but within a practical distance of drivable roads. Unburned plots were sampled in unburned islands or just outside the wildfire perimeter (Fig. 1) and served as a proxy for pre-fire fuel conditions.

2.1.2. *Monroe Mountain prescribed fires*

Three Rx fires intended as high intensity, stand-replacement fires were carried out on the Monroe Mountain (MM) unit of Fishlake National Forest in southern Utah between June 2019 and November 2020 (Fig. 1) for FASMEE. The Manning Creek Rx fire occurred on 20 June 2019 and burned 445 ha. On 7 November 2019, the Langdon Mountain Rx fire was carried out and burned 405 ha. Almost one year later, 5 November 2020, the Annabella Reservoir Rx fire burned 304 ha. FIREX-AQ flew the ER-2 aircraft with the hyperspectral sensor over MM on 21 August 2019 at high altitude, capturing post-fire fuel conditions on the Manning Creek burn and pre-fire fuel conditions on the upcoming Langdon Mountain and Annabella Reservoir burns. FASMEE measured fuels before and after the Rx burns in clustered field plots systematically laid out from a random starting point, within the prevailing forest types of subalpine fir and mature aspen encroached by subalpine fir.

2.2. *Data sets*

This study employed passive and active remotely sensed data to model and map pre-fire fuel traits where fire occurred. Ground measurements from fuel source characterization plots provided essential ground reference information on fuel characteristics and condition. Other ancillary remotely sensed data were used, such as multispectral imagery and topographic variables derived from digital elevation models, to fill in data gaps and characterize variability in the study landscapes. All gridded and raster-based data were processed using the raster and terra R packages (Hijmans, 2023a, 2023b).

2.2.1. *Imaging spectroscopy*

Airborne imaging spectroscopy data were available for each fire

(Fig. 1), from the Airborne Visible/Infrared Imaging Spectrometer Classic sensor (AVIRIS-Classic; Green et al., 1998). AVIRIS-C data were collected and provided by the NASA Jet Propulsion Laboratory for the FIREX-AQ and FASMEE campaigns. The AVIRIS-C imagery used in this study were collected before, during, or after fire and contained data gaps over the fire extent due to various constraints driven by fire activity, smoke, and planned flightlines. Images used in this analysis were selected and subset to areas that were smoke-free and reasonably close to the fire. Based on proximity, we assume unburned vegetation just outside the fire perimeter was similar to pre-fire vegetation inside the perimeter. All images were collected at approximately a 15-m spatial resolution. Three images collected during active fire were selected for model development at the WF Fire and two images for the MM Rx fires (Fig. 1).

The AVIRIS-C sensor is an airborne imaging spectrometer that samples 224 bands at an interval of 10 nm from 350 to 2500 nm (Green et al., 1998). Standard image products for the AVIRIS-C sensor were provided by NASA Jet Propulsion Laboratory including a topographic and bidirectional reflectance distribution function (BRDF) corrected surface reflectance product, equivalent water thickness, and partial least squares derived foliar functional traits (ex. carbon, nitrogen, lignin) using models from Wang et al., 2020. Poor quality bands, either in the UV, near 2500 nm, or located within strong water vapor absorption bands were removed, resulting in a 185-band subset. For comparability, images at both study sites were processed in the same manner.

2.2.2. Multispectral imagery

The subset areas for each study site were selected to cover the entire burn perimeter of the fire(s) and the AVIRIS flightlines. The Sentinel-2 imagery covered the subset area and the raster grid was used as the spatial reference for all other data and defined the spatial resolution of the modeled fuels. Multispectral imagery from ESA Sentinel-2 was used to fill spatial data gaps in the chemical trait and fractional cover maps derived from AVIRIS-C imagery over the entire burned area for the WF fire and portions of the MM Rx fires.

For the WF Fire, significant cloud cover was present in the pre-fire Sentinel-2 imagery for several collections prior to the fire. To obtain cloud-free imagery, five images were selected (four pre-fire and one during fire) to create a composite image using the median pixel value from the five images, allowing for the extremes of clouds or cloud shadows to be excluded from the composite image. The image dates selected for this fire ranged from 30 May 2019 to 18 August 2019. The goal was to obtain an image that could represent the pre-fire vegetation with no cloud cover (Fig. 2). A pre-fire composite image was used for the MM Rx fires due to cloud and snow cover before the Manning Creek Rx fire. Image dates selected for this composite ranged from 12 June 2018 to 7 June 2019.

Additionally, images were used to derive dNBR (Key and Benson, 2006). The post fire image used to calculate WF dNBR was from 2 September 2019. The post-fire image for the Manning Creek Rx fire is from 27 June 2019. The other pre-fire images were from 25 October 2019 and 24 October 2020 for Langdon Mountain and Annabella

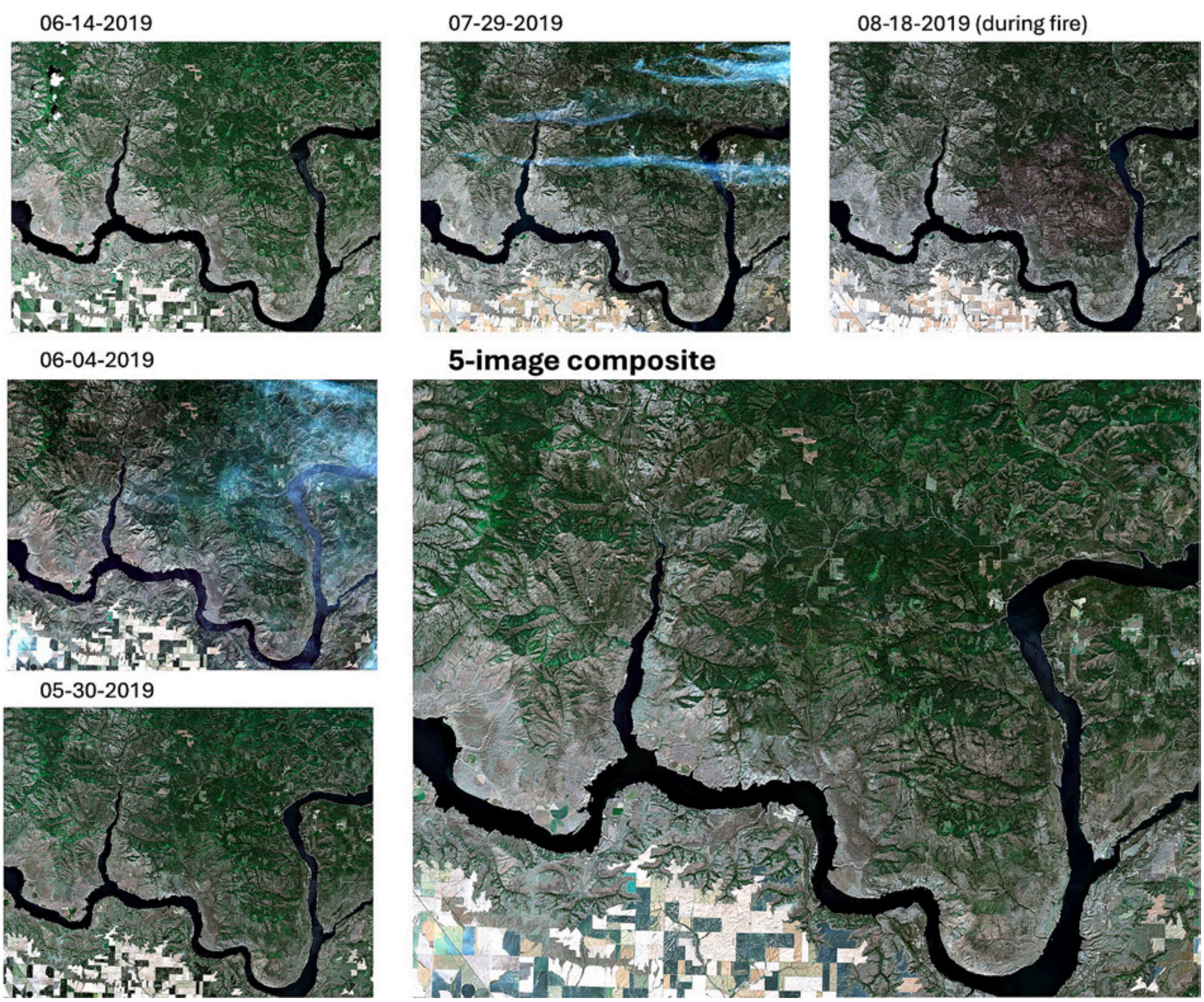

Fig. 2. Five images used to create a cloud free pre-fire mean composite Sentinel-2 image at the Williams Flats Fire location. Four pre-fire images and one mid-fire were used to create the composite due to incomplete coverage of the burn location immediately pre-fire.

Reservoir respectively. The fall Rx fires (Langdon Mountain and Annabella Reservoir) were planned to be close to potential precipitation events so the first post-fire images as close in time to post-fire with no clouds or snow used to calculate dNBR were 7 May 2020 and 11 June 2021.

The Sentinel-2 Level-2A bottom of atmosphere corrected imagery product was used in this analysis. Sentinel-2, in particular, was selected because it has a greater number of bands than Landsat to produce a relationship to map hyperspectral derived variables and a higher spatial resolution to map pre-fire fuel traits at a finer scale. Ten bands in the visible to shortwave infrared portion of the spectrum were used for this study. The red, green, blue, and NIR bands were aggregated using a simple mean from 10-m resolution to match the 20-m resolution of the remaining bands. The bands excluded from this analysis were the coastal aerosol, water vapor, and SWIR—cirrus 60-m bands. Pre-fire images were selected and used to best model pre-fire fuels. The Sentinel-2 imagery were processed using the R raster package (Hijmans, 2023a).

2.2.3. *Light detection and ranging*

The lidar signal can penetrate the canopy and provide high-resolution three-dimensional structure information throughout vegetation and fuel strata. Discrete multi-return lidar data were collected pre- and post- fire for both study sites. The point cloud data for the MM Rx fires were processed using the lidR (Roussel et al., 2020) package in R statistical software (R Core Team, 2023). The point cloud was height normalized using the normalize_height function and the k-nearest neighbor inverse distance weighting (knnidw) algorithm applied to the vendor provided digital elevation model, which removes the influence of terrain and allows for comparison of above ground measurements across the dataset. The lidar data for the WF fire were processed and identical metrics provided by the Confederated Colville Tribe.

Plot-level lidar metrics were calculated using the point cloud located within an 8-m radius of each plot center, to match the radius used in field data collection (McCarley et al., 2022). Plot-level metrics were used to train predictive models fit to response variables calculated from the field plot measurements. Gridded metrics were calculated to apply the predictive fuel characteristic models to produce continuous maps at each fire location. Descriptions of the metrics used in this study are provided in Supplemental Table 1 (Table S1). For both locations, standard vegetation metrics, using first returns for height metrics and all returns for density metrics, were computed using the height normalized point cloud for the canopy and understory. The gridded metrics were calculated at a 20-m resolution (Table S1).

For the WF Fire, the pre-fire lidar data were collected in 2014 (i.e., pre-fire) at a pulse density over 7 pulses/m^2. The post-fire lidar were collected two weeks after the fire. Due to the timing of the field data collection, the plot-level metrics used to train the models were generated from lidar collected two weeks post-fire and applied to the pre-fire gridded lidar metrics for mapping. The lidar metrics calculated for the WF Fire included canopy and understory metrics, including density (Woods et al., 2008), canopy cover, 95th percentile height, 50th percentile height of returns greater than two meters and standard deviation of the returns greater than two meters. The understory metrics included average height, 25th percentile height, 10th percentile height, and 50th percentile height of returns less than two meters. For the MM Rx fires, pre-fire lidar data were collected in leaf-on, snow-free conditions between 27 August 2016 and 11 September 2016. The pulse density averaged greater than 8 pulses/m^2.

2.2.4. *Ground-based fuels measurements*

Field measurements for fuel characterization were collected and provided by the USFS for both WF and MM.

As the WF Fire was a wildfire, field data were collected immediately after the fire from 20 to 22 September 2019 in burned and unburned areas of the fire extent (Hudak et al., in review). In total, 20 plots were collected with nine out of the total 20 being covered by AVIRIS flightlines (Fig. 1). The field sampling protocol was to collect in areas of dominant LANDFIRE Existing Vegetation Types with a minimum 30 m spacing between plots. Measurements for the fuels and ground fuels were collected along 15-m transects and for all trees within an 8-m radius of the plot center. Ground fuels measurements were recorded at 0, 6, 9, and 15 m. Because each plot center and 15-m transect was within the size of a single 20-m pixel, the transect measurements were averaged to provide a single plot value for each measurement for use alongside the gridded data. Six source characterization measurements were used in this study, including canopy top height, height to live canopy, crown base height, diameter at breast height, litter depth, and duff depth. One of the field plots (plot 3; burned) was excluded from this analysis because the measures were anomalously high for the canopy characteristics and caused inverted fuel model predictions. As well, only 18 of the 20 available plots contained canopy fuel characteristic measurements, so the canopy characteristic predictive models were developed using 17 field plots, 16 for height to live canopy, with the remaining characteristics developed using data from 19 field plots.

Field measurements were collected pre burn at all three Rx fires on MM (Eagle et al., 2024). A total of 125 plots were collected from across the three burns with 40 plots at the Manning Creek Rx burn, 25 plots at the Langdon Mountain Rx burn, and 60 plots at the Annabella Reservoir Rx burn. Because these were Rx fires, 60 of the plots were sampled before and after the burn. All plots for the Langdon Mountain and Annabella Reservoir burns are covered pre-burn by AVIRIS imagery while the AVIRIS imagery at Manning Creek includes cloud shadows and burned landscape for all plot locations. The number of plot measurements ranged from 40 to 125 plots depending on the fuel characteristic. The fuel measurement protocol was similar to WF but the plots were spaced 20.12 m (or 66 ft) apart and were selected for all plots to be within the same vegetation community. Measurements from the forest floor were collected between the plot centers located 10 m (33 ft) from plot center in the direction of the next plot center. Overstory data were collected for every other plot. Six source characterization measurements were used in this study. The measures included canopy top height, height to live canopy, crown base height, diameter at breast height, litter depth, and duff depth.

Plot-level measurements of fuel characteristics can be scaled to the landscape level as a continuous output through modeling (Pierce et al., 2012). The field plot data are essential to this study because it is necessary to use them to generate a model that produces continuous fuel characteristic maps. Field plot measurements were collected in all major fuels strata, which may allow for more accurate consumption and emissions estimates. For use with gridded remotely sensed data, the plot measurements were averaged over the plot area.

2.2.5. *Ancillary data*

Digital elevation model (DEM) data from the U.S. Geological Survey National Map 3DEP collection were used in this study as additional data to model and map pre-fire fuels. Slope and aspect data are helpful for defining fuels because they are related to vegetation composition, structure, abundance and distribution. 1/3-arc *sec* DEM data were retrieved from USGS National Map and subset, projected, and aggregated to the same grid and extent as the Sentinel-2 multispectral imagery. The data were processed to retrieve slope and aspect from the DEM. The aspect data were transformed into the Topographic Solar-Radiation Aspect Index (TRASP) where aspect ranges from zero to one (Roberts and Cooper, 1989). The TRASP scale represents the coldest and wettest aspect of zero to the warmest and driest aspect at one. The TRASP transformation allowed for the use of aspect recorded in planar coordinates, linearizing it to make it compatible with the other explanatory variables used for predictive modeling. National Agriculture Imagery Program (USDA NAIP) aerial imagery and Worldview-2 imagery were used for visual reference alongside the AVIRIS topo/BRDF product. The NAIP imagery collected at each study site has a spatial resolution of 0.6-m and Worldview-2 has a spatial resolution of

0.5-m panchromatic and 2-m multispectral.

2.3. Methodology

The methods include three steps (Figure S1):

i. derive fractional cover and estimate AVIRIS fuel trait data over the extent of the fires;
ii. build fuel characteristic models with AVIRIS (and estimated AVIRIS), lidar, and ancillary data related to ground fuel characteristic measurements;
iii. apply fuel characteristic models to the predictor data to derive continuous fuel characteristic maps.

2.3.1. AVIRIS fuel trait modeling and fractional cover

Spectral library building for fractional cover.

For this study, Multiple Endmember Spectral Mixture Analysis (MESMA; Roberts et al., 1998) was used to estimate fractional cover of green vegetation (GV), non-photosynthetic vegetation (NPV), and substrate (soil) over the burn scar. MESMA was used to identify the cover composition of a pixel by decomposing the observed spectral signature into pure reference spectra. Pure reference spectra are known as endmembers and are combined in a spectral library for application in MESMA. Multiple endmembers within the same classes included in the spectral library are used to decompose the observed spectra and estimate the fractional cover in each pixel in an image. MESMA is a variant of spectral mixture analysis in which the number and types of endmembers are allowed to vary on a per-pixel basis.

The endmember spectra used in the study spectral library are homogenous cover materials of GV, NPV, and soil. A spectral library was developed specifically for the WF Fire and for the MM prescribed burns using image-collected and field-collected spectra. NAIP and Worldview-2 were used to locate areas of homogenous cover that match the approximately 15- to 16-m resolution of AVIRIS imagery. Branch-scale field collected spectra from a field-collected spectral library from Washington state were also included to supplement the non-photosynthetic vegetation and soil classes (Roberts et al., 2004).

All collected spectra were included in a library that was optimized to create a subset that provides optimal separability between classes, while also capturing the within-class variability of each class. Based on prior analysis by Tane et al. (2018), endmembers were optimized based on the metrics of Endmember Average Root mean square error (EAR, Dennison and Roberts, 2003), Minimum Average Spectral Angle (MASA; Dennison et al., 2004), and Count Based endmember selection (CoB; Roberts et al., 2003). The EAR metric is based on root mean square error (RMSE) of the spectra where the optimum spectrum has the lowest average RMSE. The MASA metric is based on spectral angle where the spectral angle between each endmember spectrum and the other endmembers in the library is calculated. The lowest average spectral angle represents the best MASA candidate endmember. The CoB optimization metric selects endmembers for each class based on the spectrum that models the most spectra within the same class (Roberts et al., 2003).

After optimization, the resulting spectral library used for the WF Fire included 11 char, 9 GV, 10 NPV, and 7 soil endmember spectra. One GV and five NPV endmembers were included from the Roberts et al. field collected library (Roberts et al., 2004), and the rest were collected from the topo/BRDF AVIRIS imagery. The resulting library used for the MM Rx fires was developed with the same process and included 9 char, 10 GV, 8 NPV, and 4 soil endmember spectra. All 8 NPV endmembers were included from the Roberts et al. western U.S. field collected library (Roberts et al., 1993, 2004, 2006).

Spectral unmixing to derive fractional cover.

MESMA was run for all models with up to five endmember models using Viper Tools version 2.1 (Roberts et al., 2019) ENVI (Harris Geospatial Solutions, Broomfield, CO, USA) extension. The AVIRIS topo/BRDF images were unmixed with the optimized spectral library. Additionally, for areas not covered by the AVIRIS imagery, we convolved the spectral libraries to unmix the Sentinel-2 imagery. The possible models for each pixel were set to include two to four endmembers from different functional classes, including shade for the images unmixed without char fractions and burn scar, and two to five models for the images that included partial burn scar. The settings selected for running MESMA include a minimum allowable endmember fraction of 0.00 and a maximum of 1.00. The minimum allowable shade fraction was set to 0.00 and the maximum was set to 0.8. The maximum allowable RMSE was 0.025 and the multiple-level fusion RMS threshold was 0.007. After running MESMA, the unmixed fraction images were shade normalized where surface material abundance is estimated without the influence of shade (Adams et al., 1993).

Fuel trait modeling.

Due to data gaps in the spatial coverage of the available AVIRIS imagery, Random Forests (Breiman, 2001) regression was used to estimate pre-fire AVIRIS plant chemical traits. The candidate predictor variables included all Sentinel-2 multispectral bands listed, alongside elevation, aspect, and slope data, with each AVIRIS fuel trait as the response variable for the Random Forests regression. Random Forests regression was selected as the method for modeling these data because it is a non-parametric method that accommodates the distributions of vegetation trait data and produces a continuous model that does not extrapolate beyond the range of values in the training data (Breiman, 2001). Random Forests regression is a supervised machine learning algorithm that uses an ensemble of trees representing various regressions with a randomly selected predictors at each node of the tree. By developing the ensemble in this way, Random Forests is robust to noise or outliers (Breiman, 2001). Predictive models of AVIRIS chemical traits were trained using a random spatial sampling of 1000 points for each model. To obtain a sample that represented pre-fire vegetation, the sampled area excluded burn, active fire, water (lakes, reservoirs, rivers), clouds, or cloud shadows. A total of five models were produced for the traits of equivalent water thickness, carbon, leaf mass per area, lignin, and nitrogen. The models were developed in R statistical software (R Core Team, 2023) using the randomForest and raster packages (Liaw and Wiener, 2002; Hijmans, 2023a). Regression models were selected with “rf.modelSel” from the rfUtilities package (Evans and Murphy, 2019). The hyperparameters selected to build each regression model was with 500 trees (ntree = 500) and four variables tried at each split determined by the total number of candidate predictor variables divided by three (p/3). The predictive models were assessed by implementing a permutation test cross-validation with “rf.crossValidation” from the same R package. The models were then applied to derive maps of AVIRIS chemical traits and equivalent water thickness covering the burn areas.

2.3.2. Model building and performance

Partial least squares regression (PLSR) was selected to model spatially continuous heterogenous fuel characteristics. PLSR models were developed for each fuel characteristic at each study site. PLSR is often used for prediction and mapping of biophysical variables using a combination of field data and imaging spectroscopy data (Serbin et al., 2014; Singh et al., 2015). The models were built using in situ fuel characteristics as the response variables and chemical traits, fractional cover estimates, canopy and understory lidar metrics, Sentinel-2 spectra, and topographic data as predictor variables (Fig. 3; Table S1 and S2). A commonly reported reason for selecting PLSR is because it is a technique that can incorporate data with high dimensionality and collinearity (Höskuldsson, 1988; Garthwaite, 1994) inherent in remotely sensed and especially spectroscopy data (Wold et al., 2001). PLSR produces components, that maximize covariance between predictor and response variables (Wold et al., 2001) rather than directly utilizing the precise numerical values of the predictors. We determined the optimal number of components, with 200 jack-knifed splits of the data, by minimizing the root mean square error (RMSE) of the predicted residual sum of

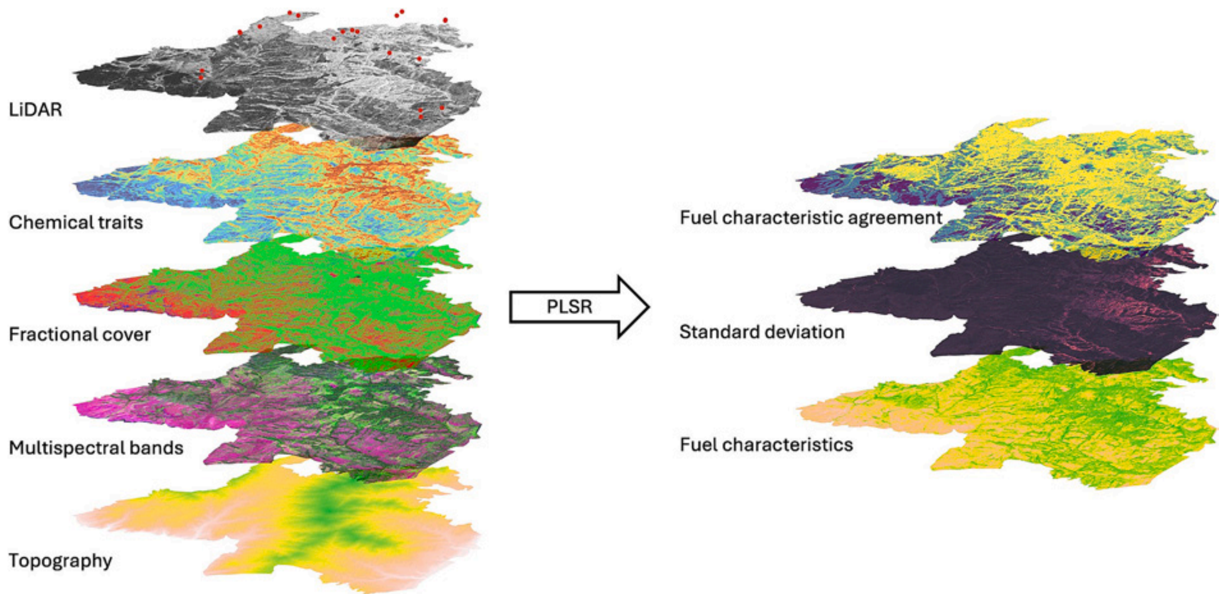

Fig. 3. Variables used to predict for fuel characteristics with partial least squares regression (PLSR). The model is then applied to the same data to map pre-fire fuel characteristics. Maps of standard deviation of the model estimates that represent uncertainty are also produced and masks of high confidence fuel characteristic values that are combined for all characteristics to show the spatial distribution of a high confidence agreement of fuel characteristic estimates.

squares (PRESS) statistic (Wold et al., 2001) with no significant improvement in RMSE of the following components using a *t*-test (Serbin et al., 2014). Following PLSR based approaches like Singh et al. (2015) and Wang et al. (2020), the data for each fuel characteristic were separated into calibration and validation sets with a 70/30 % split. The calibration data were further permuted to build 200 separate PLSR models using 70 % of the calibration data to train the model for each permutation. The resulting 200 PLSR models were applied to calculate mean and standard deviation of the predictions for each fuel characteristic. Using averaged predictions of the PLSR models enables estimates of uncertainty at a pixel scale. We used the coefficient of determination (R^2) and root mean square error (RMSE) of the calibration and validation sets to assess model performance. Additionally, we range normalized the RMSE (NRMSE) to compare error between all fuel characteristic models and separated RMSE into systematic and unsystematic error (RMSEs and RMSEu respectively).

To understand the contribution and importance of each predictor variable used in the fuel characteristic models, we use the mean standardized coefficients from the 200 PLSR models alongside Variable Influence on Projection (VIP). VIP is a summary value of the importance of a predictor variable for both the predictor and response variables (Wold et al., 2001).

2.3.3. *Fuel characteristic mapping*

The 200 PLSR models were applied to each fire location to produce predicted mean and uncertainty (standard deviation) maps of each fuel characteristic. To ensure the predictions are reasonable given the training data, we evaluated map confidence as a percentage of the mean predictions of each fuel characteristic that fell within a reasonable range of values. The range of values is the range of field collected data with bounds of 25 % beyond the minimum and maximum values in the field measurements (Verrelst et al., 2016; Wang et al., 2020). To identify the pixels and spatial patterns of the high confidence predictions, we generated binary masks to indicate the location of high confidence predictions for each fuel characteristic. The suite of fuel characteristics we present would likely be used concurrently to model fire effects such as smoke emissions. Thus, the masks were also considered concurrently to identify the locations and number of fuel characteristics with high confidence values. We summed the masks of high confidence for each fuel characteristic to create high confidence fuel characteristic agreement maps that show the number of fuel characteristics with high confidence values for any pixel and indicate locations where concurrent use of the fuel characteristics have high confidence for analysis of fire effects. We then compared dNBR and lidar-derived fuel consumption maps with the agreement map to evaluate if the estimates generated by the fuel characteristic models are confident where fire effects occur. Thus, the models can produce maps of fuel characteristics that could be spatially and concurrently meaningful in the context of fire effects modeling.

3. Results

3.1. *Fuel trait RF model performance*

The performance statistics for the Random Forests regression estimated foliar function trait maps are shown in supplementary materials and summarized in Table S3. The median permuted R^2 values from the cross validation for all chemical traits ranged between 0.53 and 0.78 for the WF Fire and 0.45 and 0.65 for the MM Rx fires. The NRMSE values were all at or below 20 % with a range of 17 % and 19.8 % for the MM Rx burns and 8.2 % to 19.9 % for the WF Fire. The NRMSE values were relatively comparable between models for each trait and for each location. The models with a larger difference in NRMSE between locations were equivalent water thickness and carbon, which had lower NRMSE values for models developed at the WF location. Percent bias for all models and locations except for equivalent water thickness for MM was 1 % or under but overall low. This indicates there is no particular tendency for the modeled values to be greater or less than the observed values.

3.2. *Fuel characteristic PLSR model performance*

The performance statistics for the models developed using the WF Fire data are shown in Table 1 and Fig. 4 and the model scatterplots are in Figure S2. The calibration R^2 values for the models ranged from 0.167 to 0.664. Calibration NRMSE was more varied and ranged from 12.42 % to 29.12 %. The validation R^2 values ranged from 0.05 to 0.75 with NRMSE values that ranged from 7.43 % to 49.83 %. The ground fuel characteristics of litter depth and duff depth performed very poorly in validation with R^2 values of 0.22 and 0.05 and NRMSE of 35.05 % and

Table 1
Summary statistics of the Williams Flats Wildfire fuel characteristic model means developed using PLSR with imaging spectroscopy and LiDAR data.

		Williams flats wildfire fuel characteristics					
		Litter Depth (mm)	Duff Depth (mm)	DBH (cm)	CBH (m)	Height (m)	Height to LC (m)
Training	min	0.25	0	14	0.23	6.9	1.7
	max	30.75	112	46.1	9.48	36.2	15.06
	mean	8.40	18.85	28.38	2.69	18.68	6.97
	SD	10.85	35.74	12.10	2.50	8.44	3.80
	N	17	17	17	17	17	16
	cal	12	12	12	12	12	11
	val	5	5	5	5	5	5
	train %	71	71	71	71	71	69
Calibration	ncomp	2	3	3	3	4	6
	R2	0.21	0.17	0.56	0.61	0.66	0.59
	RMSE	8.88	16.60	7.15	1.42	3.64	2.58
	bias	2.91	−5.68	−3.22	−0.28	−1.34	0.26
	NRMSE	29.12	14.82	22.26	15.37	12.42	19.29
	RMSEu	4.46	15.46	4.50	1.10	3.24	1.50
	RMSEs	7.68	6.04	5.55	0.90	1.66	2.09
	d	0.66	0.51	0.85	0.87	0.91	0.83
Validation	R2 val	0.22	0.05	0.57	0.68	0.75	0.70
	RMSE val	10.69	55.81	5.28	1.56	4.82	0.99
	bias val	6.55	43.69	−2.49	−0.47	−0.84	−0.15
	NRMSE val	35.05	49.83	16.44	16.91	16.44	7.43
	RMSEu val	2.67	20.40	4.10	0.61	2.38	0.74
	RMSEs val	10.35	51.95	3.32	1.44	4.19	0.66
	d val	0.66	0.64	0.87	0.87	0.90	0.88

49.83 % respectively. This is likely due to the timing of field data collection and generally lower duff and litter depth values in this region. Validation statistics for canopy related fuel characteristics were better and ranged from 0.57 to 0.75 alongside NRMSE that ranged from 7.43 % to 16.91 %. Validation systematic RMSEs were higher than unsystematic RMSEu for all models except height to live canopy and diameter at breast height, indicating systematic error that is not random and is likely due to the respective model and data. However, the low sample sizes for calibration and validation likely contribute to the magnitude of error in the models. The average difference between calibration and validation R^2 values for canopy related characteristics is 0.068 with 5.80 % difference in NRMSE. For ground fuel characteristics the R^2 difference is 0.064 and 20.47 % NRMSE.

The fuel characteristic model performance statistics for the MM Rx fires are shown in Table 2 and Fig. 4. The calibration R^2 values for all traits ranged between 0.37 and 0.72. Calibration NRMSE values ranged between 10.81 % and 18.22 %. Validation R^2 values ranged between 0.35 and 0.63 with NRMSE values between 12.67 % and 21.99 %. The validation accuracy is moderate with NRMSE values around or below 20 %. Predictive accuracy was best for top height with a higher calibration R^2 value of 0.72 alongside 11.09 % NRMSE and a validation R^2 value of 0.56 with NRMSE of 14.76 %. Generally, the performance statistics from training to validation were relatively stable for most models developed using the MM Rx fuels data. This is exemplified by an average difference between calibration and validation R^2 of 0.103 and NRMSE of 4.55 %.

The calibration and validation unsystematic error (RMSEu) values were higher for canopy top height, litter depth, diameter at breast height, and crown base height. This indicates that errors in model prediction are likely not systematic (model) errors, but rather random. Height to live canopy has a higher calibration RMSEu value than the RMSEs, but both height to live canopy and duff depth have validation RMSEs values that are higher than the corresponding RMSEu, indicating that the error is more likely due to systematic model error.

For all models at both locations, the optimum number of components used to build the model remained low, an expected behavior of PLSR models (Ahn and Bae, 2022), and ranged from 2 to 5.

for the MM Rx fire fuel characteristic models and 2 to 6 for the WF Fire models. Standardized model coefficients by variable are shown in Fig. 5 and variable influence on projection (VIP) values by variable are shown in Fig. 6.

3.3. Fuel characteristic maps and map confidence

Fuel characteristic maps for all fuel characteristics and burn locations are provided in Figure S3 and the associated standard deviation uncertainty maps are provided in Figure S4. Trait maps for the Annabella Reservoir fire location and the associated MM performance scatterplots are shown in Fig. 7. The fuel characteristics with the greatest uncertainty in predictions (Figure S4) are the ground characteristics of litter and duff depth (Fig. 7). The area of the fuel characteristic maps with high confidence values ranged from 76.36 % to 92.44 % for WF Fire and above 94.5 % for all characteristics for the MM Rx fires (Table 3). The areas with the greatest overlap, or agreement, of high confidence fuel characteristics are not proportional as all fuel characteristic maps have a high percentage of high confidence values (Table 3) and thus greater agreement amongst all traits. As well, when compared to a map of burn severity using the differenced Normalized Burn Severity index (dNBR), the areas with the most agreement of fuel characteristics with high confidence also covered the greatest range of burn severity classes (Fig. 8; Figure S5). In turn, the areas with the least agreement covered the lowest range of burn severity classes. When compared to lidar derived total fuel consumption maps (McCarley et al., 2024), we also see the areas with the most agreement covered the greatest range of fuel consumption for MM Rx fires. The WF Fire covers a large range in consumption values for areas with agreement amongst all fuel characteristics but areas of less agreement (four fuel characteristics) cover the greatest range of fuel consumption values (Fig. 9; Figure S6). The same holds true that areas with the least fuel characteristic agreement cover areas with lower fuel consumption.

4. Discussion

We developed a methodology to provide spatially heterogenous continuous fuel characteristic maps with uncertainty using imaging spectroscopy and lidar data by calibrating and validating PLSR models using field measures of fuels. We demonstrate imaging spectroscopy paired with lidar is capable of consistently and accurately capturing spatial variability in pre-fire fuel characteristics that are necessary for relating fuels to fire emissions. The framework for employing imaging spectroscopy and lidar data produced consistent results and error when applied to multiple scenes for both wildfires and Rx crown fires.

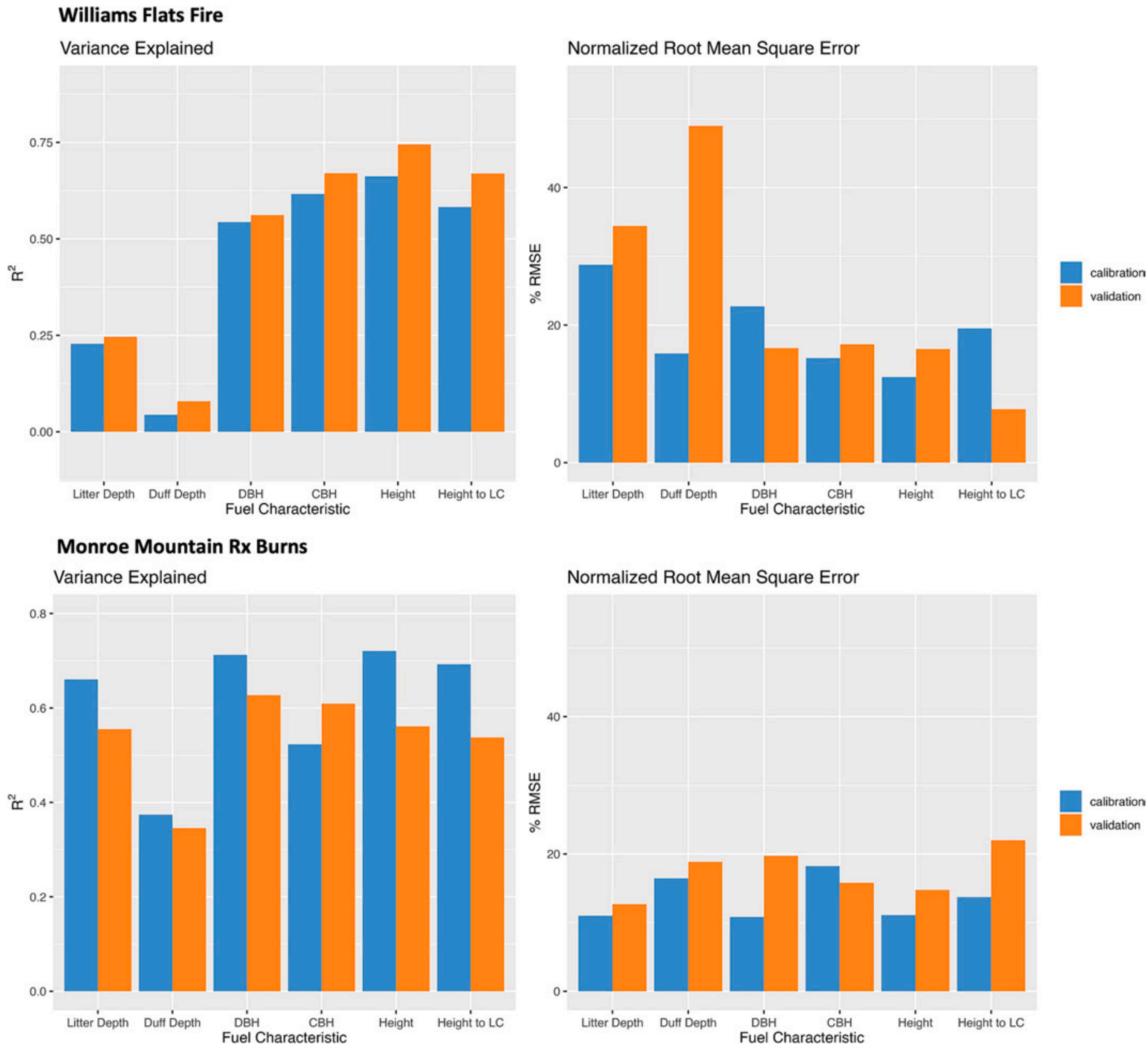

Fig. 4. Model calibration and validation variance explained (R^2) and normalized root mean square error (NRMSE) for both fire locations.

Partial least squares regression using data permutation for uncertainty analysis has been successfully employed for mapping a variety of foliar functional traits with imaging spectroscopy across biomes and time (Singh et al., 2015; Wang et al., 2019; Wang et al., 2020; Burnett et al., 2021) but has not been explored to continuously map pre-fire fuel characteristics for fire effects modeling. To the extent of methodological comparison to the outcomes of those studies, we modeled and mapped fuel characteristics with generally consistent error, around or under NRMSE of 20 %, and detailed uncertainty statistics at multiple locations (Tables 1 & 2). NRMSE values lower than 20 % meet the requirements for large area mapping of foliar functional traits (Asner et al., 2015; Moreno-Martínez et al., 2018; Wang et al., 2020), indicating the methods of this study have the potential for broader application. Our study provides a continuous estimation of broadly applicable fuel characteristics with uncertainty that more directly relate to fire effects.

4.1. *Interpretation of fuel characteristic models*

Overall, the models indicate the fuel characteristic modeling and mapping methodology is capable of achieving consistent results with low error. The canopy related fuel characteristic models performed well. When compared, the calibration and validation sets resulted in similar error with average differences of 5.81 % and 4.61 % for all canopy fuel characteristics at the WF wildfire (Table 1) and MM Rx burns (Table 2) modeling locations respectively. Duff depth did not perform well between the calibration and validation sets and between the two modeling locations. Litter depth had similar performance to duff depth for the WF wildfire but performed as well as the canopy fuel characteristic models for the MM Rx burns. The performance of the ground fuel characteristic models for WF Fire are likely explained by the limited sample size ($N = 17$, Table 1), which includes burned and unburned plots. The poorer performance of ground fuel characteristic models is consistent with other studies focused on ground-based fuels across a variety of ecosystem types (Jakubowksi et al., 2013; Bright et al., 2017; Alonso-

Table 2
Summary statistics of the Monroe Mountain Rx Burns fuel characteristic model means developed using PLSR with imaging spectroscopy and LiDAR data.

		Rx Burns Fuel Characteristics					
		Litter Depth (mm)	Duff Depth (mm)	DBH (cm)	CBH (m)	Height (m)	Height to LC (m)
Training	**min**	0.00	−2.25	15.72	0.30	7.93	0.35
	max	46.38	146.75	32.19	8.11	18.91	8.16
	mean	14.21	54.44	21.74	4.33	12.13	5.08
	SD	9.237	31.15	4.078	2.060	2.376	2.155
	N	125	105	40	40	40	40
	cal	88	74	28	28	28	28
	val	37	31	12	12	12	12
	train %	70.40	70.48	70	70	70	70
Calibration	**ncomp**	5	3	5	2	5	3
	R2	0.66	0.37	0.71	0.52	0.72	0.69
	RMSE	5.10	24.50	1.78	1.42	1.22	1.07
	bias	−0.359	−0.385	0.110	−0.010	0.043	0.069
	NRMSE	11.00	16.44	10.81	18.22	11.09	13.71
	RMSEu	4.34	14.34	1.29	1.01	0.94	0.84
	RMSEs	2.68	19.86	1.23	1.00	0.78	0.66
	d	0.89	0.71	0.90	0.82	0.91	0.89
Validation	**R2 val**	0.56	0.35	0.63	0.61	0.56	0.54
	RMSE val	5.88	28.10	3.25	1.23	1.62	1.72
	bias val	−0.580	2.343	−0.035	−0.204	0.054	−0.820
	NRMSE val	12.67	18.86	19.72	15.81	14.76	21.99
	RMSEu val	5.46	13.03	2.31	1.10	1.30	0.82
	RMSEs val	2.16	24.90	2.29	0.56	0.97	1.51
	d val	0.88	0.68	0.86	0.88	0.85	0.78

Rego et al., 2021). The spatial variability of duff and duff consumption is not well understood and is variable at fine scales (Miyanishi, 2001; Keye et al., 2014). The same is true for litter and the fine scale spatial variability of ground fuel characteristics such as litter and duff likely limits the performance of the models produced in this study. The performance of the litter depth model for the MM Rx burns could be attributed to the ground data because it was collected pre-fire. Additionally, the number of litter samples across three Rx burn areas of MM ($N = 125$) and the systematic plot spacing strategy could capture heterogeneity in the distribution more consistently.

The remote sensing model variables were selected, in part, to represent fuel variability using the biophysical relationships observed through remotely sensed data rather than operational or purely conceptual applications of remotely sensed data (Gale et al., 2021). The standardized model coefficients shown in Fig. 5 and variable influence on projection (VIP) values shown in Fig. 6 illustrate the remote sensing variables and by extension the biophysical relationships that the fuel characteristic models rely on. Variables from all variable groups were used to estimate fuel characteristics. The variables used represent reasonable and relevant biophysical relationships between the remote sensing data and the ground-based fuel characteristic measures.

For VIP values, a value of 0.8 or greater is considered to be a variable that is highly influential for the fuel characteristic model (Wold et al., 2001; Burnett et al., 2021). For example, the lidar variables used by the ground fuels characteristic models included understory variables such as standard deviation of understory returns, 50th percentile of understory returns, and average of understory returns. Similar to Labenski et al., 2023, we found the influential remotely sensed predictor variables for estimating litter and duff are those that capture canopy properties such as canopy lidar metrics rather than understory variables alone (Figs. 5 and 6). The WF 10th percentile lidar height returns did not contribute to any models as the plot-associated values were zero or near zero. The same variable was not influential (VIP under 0.8) for litter and duff in the Rx burn models, though, understory cover, 25th, and 50th percentile of height returns were influential understory predictor variables for duff and litter for both locations. As well, canopy variables that were used such as density and cover and overstory correlates have been documented as useful for predicting ground fuels using lidar (Bright et al., 2017, 2022; McCarley et al., 2020; Price and Gordon, 2016; Stefanidou et al., 2020).

For the imaging spectroscopy variables, the nitrogen chemical trait was a highly influential predictor for all fuel characteristic models at both study sites including the canopy fuel characteristics which are structure-based measurements. This could be due to the role of foliar nitrogen as an important component for both photosynthesis and the structural development of plants. As well, foliar nitrogen and LMA are also related to decomposition of both canopy foliage and litter (Chapin and III., 2003; Kazakou et al., 2006; Quested et al., 2007; Santiago, 2007). Both are considered influential for prediction in the duff depth models at both study sites. However, LMA is just under the influential value (VIP = 0.79) for the WF litter model which could also be explained by the smaller number of field measurements made across unburned and burned plots.

Fractional cover of green vegetation is consistently influential for the models related to canopy structure, specifically for crown base height and height to live canopy for both study sites. Lignin is influential for the duff depth models of both study sites. Lignin is resistant to decomposition and this relationship may attribute to its influence in the models as high lignin content can lead to deeper layers of duff. Carbon content is an influential variable in all of the MM fuel models but only for the litter and duff depth models of WF. Carbon content is a trait with less natural variability (Singh et al., 2015) that could affect its influence in the model due to the trait range in the input imagery or the Random Forests modeling of the trait.

The overall variability in VIP values for the chemical traits between sites and fuel characteristics could be due to factors of plant functional types, site productivity, or variation in the input data. The contribution of the imaging spectroscopy derived variables to the fuel characteristic model predictions indicates known biophysical relationships and processes in vegetation. Thus, imaging spectroscopy and lidar have potential for use to continuously map fuel characteristics.

Additionally, spectral variables in the vegetation red edge through SWIR multispectral bands were influential for all fuel characteristics. The visible spectral bands, however, provided less consistent influence on the prediction of fuel characteristics as they were not all influential contributors to the prediction of fuel characteristics at the WF Fire but were important for the MM Rx fires (RGB VIP > 0.8 for all fuel characteristics). The VIP plots for corresponding fuel characteristics at each study site do not particularly align in the areas of highest contribution to the prediction of those characteristics. This could be due to ecoregional

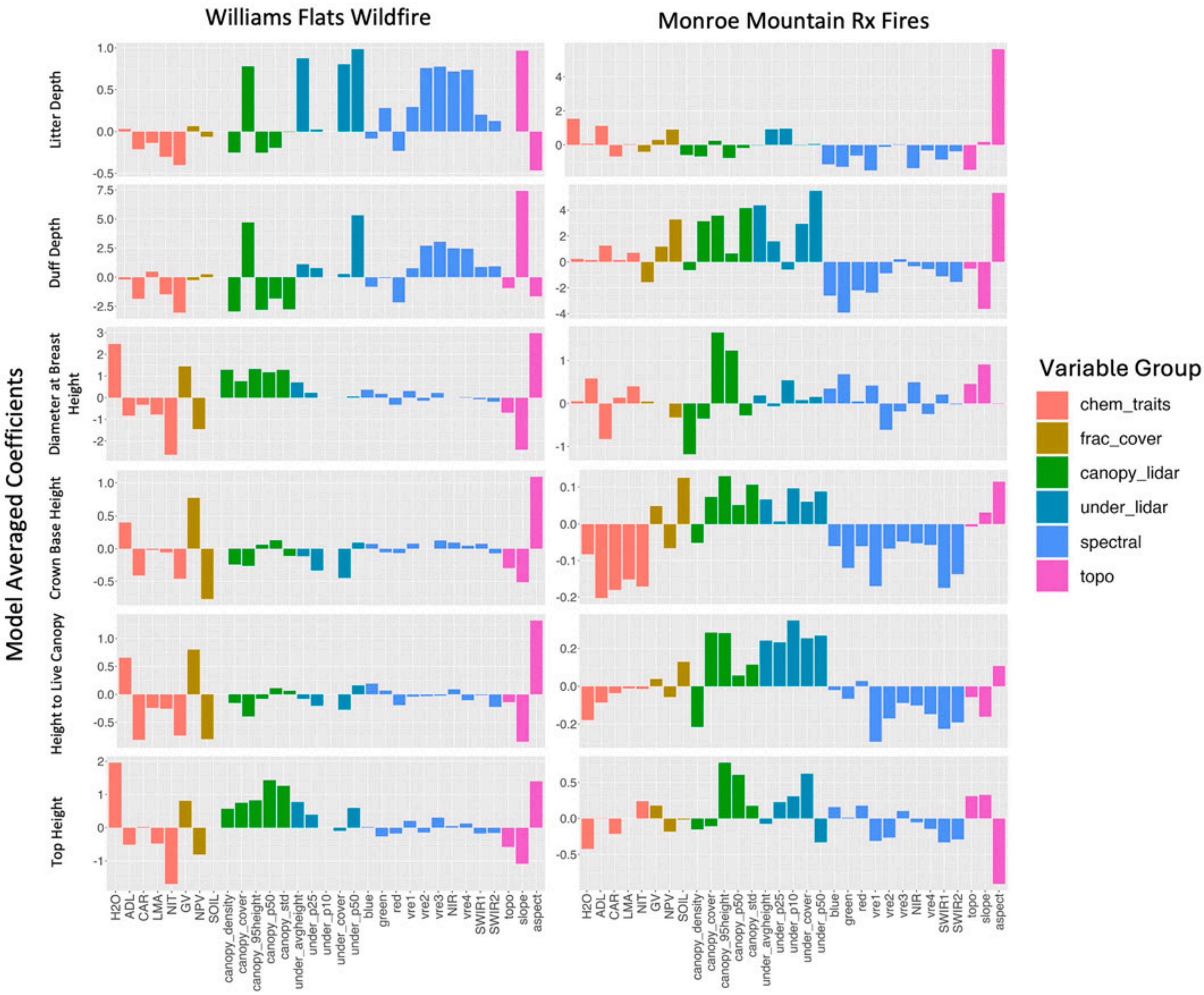

Fig. 5. Model averaged standardized coefficient plots by model and study site. Standardized model coefficients put the model coefficients in terms of standard deviation.

differences or other variation captured in the field measured data.

The coefficient plots for the canopy fuel characteristic models for the MM Rx burns (Fig. 5) do not display a high degree of high-frequency variation in the standardized coefficients, which can be an indicator of models that are overfit (Asner et al., 2014; Burnett et al., 2021). As well, most of the standardized coefficients for each fuel characteristic are within one to two standard deviations and thus not displaying high-frequency variation that can point to models that could be generalizable at scale. However, the duff depth model, displayed a high degree of high-frequency variation but this could be attributed to the weaker performance of the duff depth models in comparison to the other fuel characteristic models. Due to the discrepancies between standardized coefficients for corresponding fuel characteristics at each fire location, it is unclear whether the model coefficients could be transferrable to other geographic and ecoregional extents. We plan to further explore this by applying these methods to a variety of datasets in the future.

4.2. Fuel characteristic maps

Our analysis and methodological framework is focused on capturing fuel variability by continuously mapping fuel characteristics across the landscape suitable for consumption and emissions models while providing a suite of uncertainty statistics that can inform the use of fuels data in connecting it to estimates of emissions. The model averaged fuel characteristic maps for the Annabella Reservoir Rx fire are shown in Fig. 7 and Figure S3 and the standard deviation, or uncertainty, maps are shown in Figure S4. The fuel characteristic maps and uncertainty maps provide a means to estimate fire emissions and other fire effects at the landscape scale.

Because the training data are relatively limited and the collection of that data was not specifically carried out for this analysis, there are extrapolated and erroneous predictions for some areas of the fuel characteristic maps. These areas are indicated on the uncertainty maps as areas with higher standard deviation values (Figure S4) but are also mapped through confidence maps that show the locations of fuels that are constrained by the empirical data (fuels with high confidence estimates) (Fig. 7; Figure S5). Considering the spatial gaps in the imaging spectroscopy data coverage, the patterns of low confidence in the modeled fuel characteristic estimates do not specifically align with the locations of the data gaps (Fig. 1). However, for the WF Fire, the maps of standard deviation show greater model uncertainty where there are gaps (Figure S4). High standard deviation values indicate greater variation

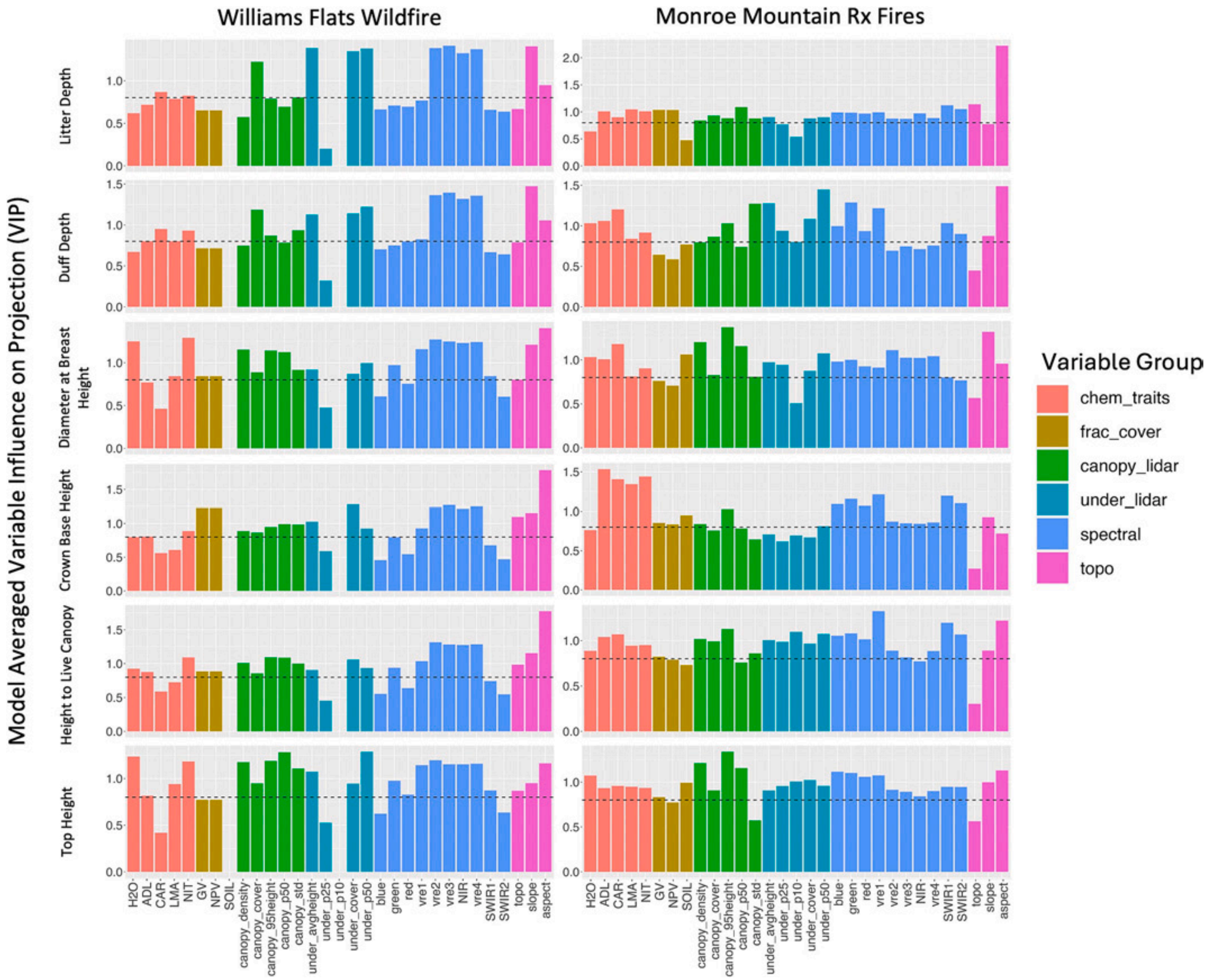

Fig. 6. Model averaged Variable Influence on Projection (VIP) plots by model and study site. VIP is a summary value of the predictor variable for both the predictors and fuel characteristics. Values of 0.8 (dashed line) or greater indicate a variable that is highly influential for the fuel characteristic model.

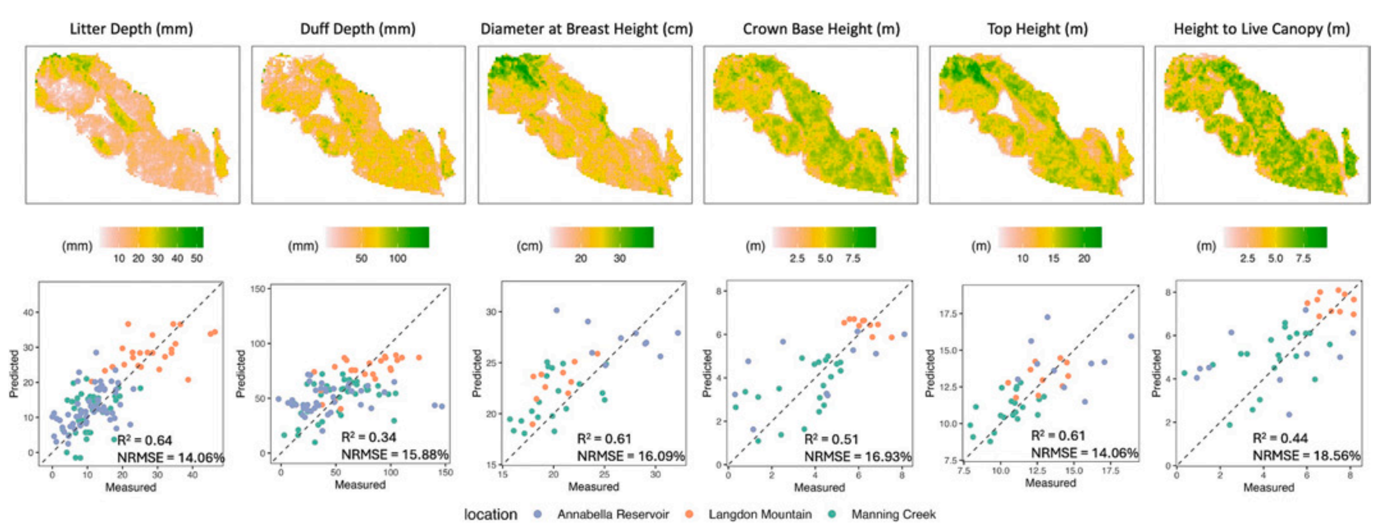

Fig. 7. High confidence fuel characteristic maps for the Annabella Reservoir prescribed burn location and associated scatterplots of all prescribed burn locations on Monroe Mountain in Utah, USA. The Annabella Reservoir location had full coverage of the fuel characteristic ground plots and burn area with predictor variable imagery. Each pixel in each map represents an average of the predictions made by all PLSR models developed using permutations of the training data.

Table 3
Percent of map with high confidence values for each fuel characteristic map by fire. High confidence values are calculated as the range of field collected data with bounds of 25 % beyond the minimum and maximum values.

		Fuel Characteristic					
		Litter Depth	Duff Depth	DBH	CBH	Height	Height to LC
Fire	Williams Flats	92.44	83.53	84.87	76.36	83.52	79.90
	Annabella	98.10	97.82	99.79	98.41	98.44	97.51
	Manning	98.66	95.58	99.64	98.69	94.50	97.18
	Langdon	98.81	96.32	99.91	98.96	98.12	97.32
	All Monroe Mtn	97.29	92.43	99.55	97.52	93.12	94.58

across the iterated model predictions. Thus, the higher standard deviation values in the imaging spectroscopy gaps signal the influence of the imaging spectroscopy derived predictors and their uncertainty in the fuel characteristic models and maps. The notably smaller gaps in AVIRIS coverage for the MM Rx burns do not show the same uncertainty in standard deviation. When visually compared to the imagery and lidar, the areas that lack high confidence estimates are often where the vegetation do not possess the measured characteristics being modeled (e.g. grasses). In this case, these high confidence maps can be used as a mask to select and maintain only the areas with values that are considered high confidence. The maps of the MM Rx fires are mostly covered by high confidence values and the WF Fire have lower percentages of high confidence values (Table 3). This may be because the WF wildfire was much larger with a greater range of fuel conditions yet represented by a sparser field plot sample compared to the MM Rx fires. On the other hand, it can also be argued that the WF field plots (collected in only three days) more efficiently sampled the wildfire burn area, whereas the clustered MM field plots may not have captured as well the broader, landscape-level range of fuel conditions.

When the fuel characteristic agreement maps are compared to differenced normalized burn ratio (dNBR), we see at all fires that the areas that did not have high fuel characteristic agreement and high confidence estimates covered lower severity or unburned locations (Fig. 8; Figure S5). When compared to total fuel consumption maps (Fig. 9; Figure S6), a similar pattern exists where areas of lower consumption cover areas with fewer high confidence estimates. Thus, areas where all or most fuel characteristic maps have high confidence values cover the greatest range of burn severity values and a large range of fuel consumption. The MM Rx fires were crown fires lit by a helitorch which resulted in more homogenously severe fire effects across similar

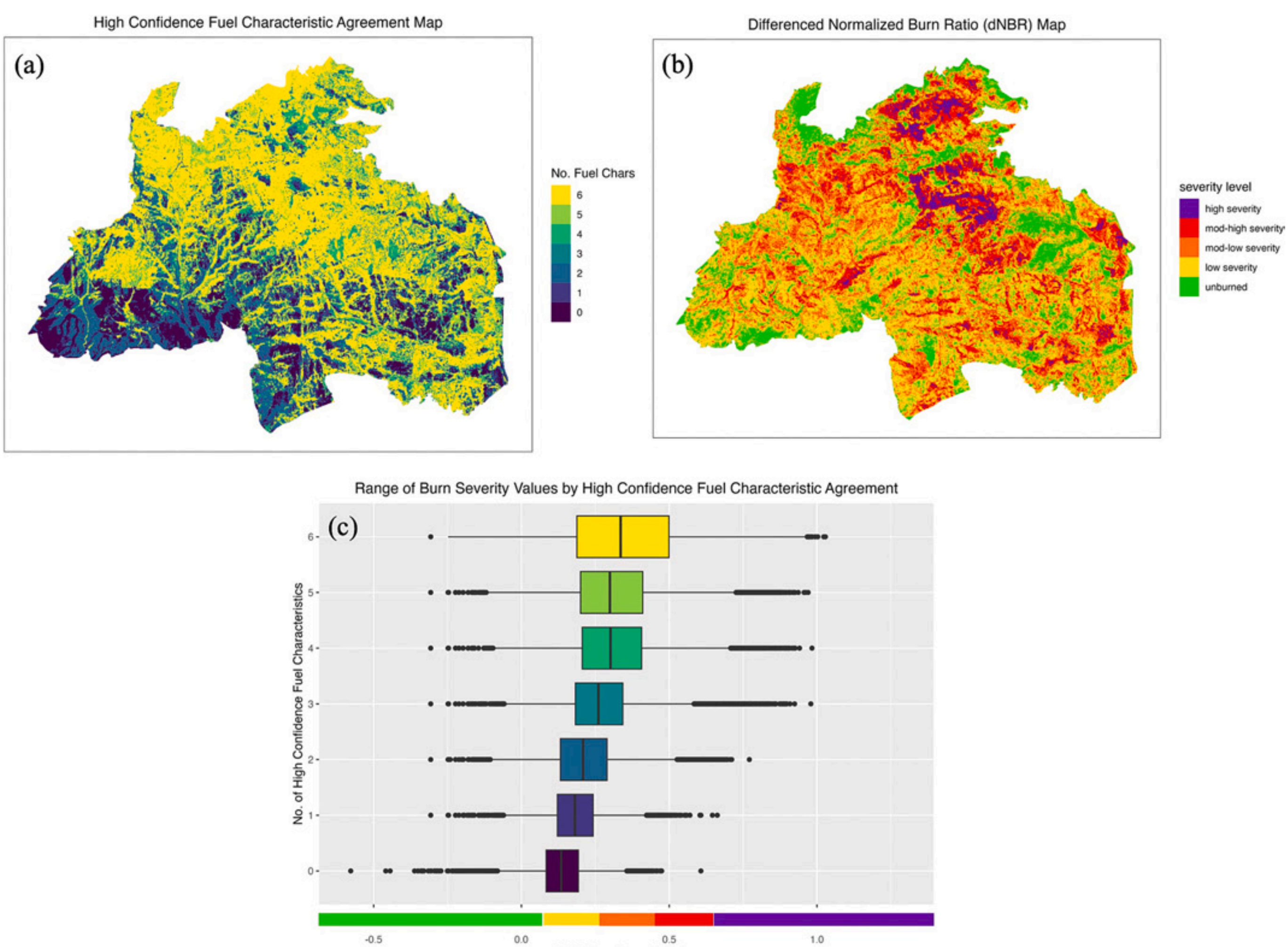

Fig. 8. Maps of the spatial distribution of high confidence fuel characteristic predictions (a) and the differenced normalized burn ratio burn severity map (b) as a guide for the associated boxplot distribution of differenced normalized burn ratio (dNBR) values for each level of agreement (c). The dNBR map was produced using pre- and post-fire NBR generated using Sentinel-2. The areas with the greatest number of traits with high confidence values capture the greatest range and levels of burn severity indicating meaningful use of the fuel characteristic maps for emissions estimates. Values 0–6 indicate the number of fuel characteristics that are considered to have high confidence predictions meaning within a reasonable range of the measured values.

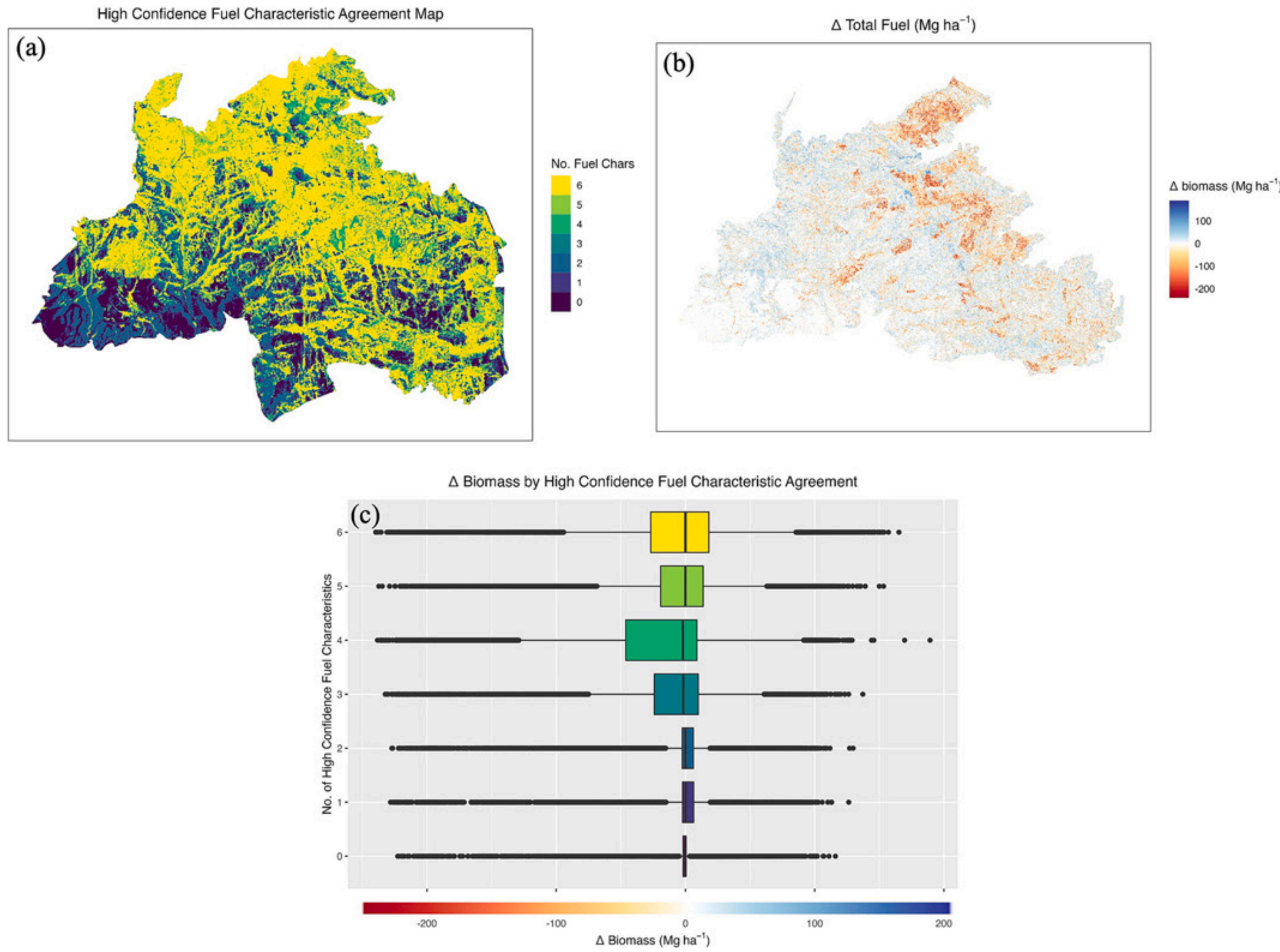

Fig. 9. Maps of the spatial distribution of high confidence fuel characteristic predictions (a) and the change in total fuel biomass (b) as a guide for the associated boxplot distribution of biomass change values for each level of agreement (c). The biomass change map was produced using pre- and post-fire lidar at each fire location following McCarley et al., 2024. The areas with the greatest number of traits with high confidence values capture the greatest range and levels of consumption indicating meaningful use of the fuel characteristic maps for emissions estimates. Values 0–6 indicate the number of fuel characteristics that are considered to have high confidence predictions meaning within a reasonable range of the measured values.

vegetation. Therefore, a much larger proportion of the MM Rx crown fires burned at high severity than the mixed severity patterns observed at the WF wildfire. For the MM Rx fires, the comparison of the agreement maps with dNBR and consumption represent the ideal that models generate confident estimates of fuel characteristics that cover the entire burn area and across all burn conditions. While the fuel models were developed for fire effects modeling, they are derived from independently collected field and remote sensing data rather than calibrated to match specific fire outcomes. The purpose of this comparison is not to establish a deterministic relationship between fuels and fire effects but rather to evaluate where the models constrain fuel characteristics well using empirical data. This indicates that the models confidently estimate fuel characteristics in areas critical for fire effects modeling—where fires occur and across a range of fire conditions. Additionally, the consumption maps quantifying fuel density (Mg ha^{-1}) and associated uncertainties have direct interpretability and applicability to carbon pool assessments and carbon flux (emissions) models, whereas unitless dNBR maps are qualitative and subject to looser interpretation.

4.3. Role of imaging spectroscopy and lidar data

The use of imaging spectroscopy data in this study was not through the direct use of detailed narrowband spectra as is typical; instead, it is used to inform the mapping of vegetation traits relevant for fuels characterization. The RF models of the functional traits for both the wildfire and Rx burn locations performed generally well with moderate R^2 values (0.4561 and 0.7872; Table S3) and low bias and error under 20 %. The RF models for the MM Rx burns did not perform as well as those at the WF Fire. However, two of the Rx burns had complete image coverage over the plot data and complete (Annabella Reservoir Rx burn) or majority coverage (Langdon Mountain Rx burn) over the burned area and thus were not modeled with random forests. The chemical trait models from Wang et al. (2020) applied to the imaging spectroscopy data have a range of validation R^2 values of 0.47 to 0.77. The performance of these models is important to take into consideration alongside the RF models for model and map uncertainty (Table S4). For example, although the RF regression R^2 is moderate, the Wang et al. (2020) lignin models applied to the imaging spectroscopy data have lower R^2 ($R^2 = 0.47$). Thus, the uncertainty in capturing the variation in lignin from the imaging spectroscopy data may propagate to the RF model and predictions. Chemical features related to the imaging spectroscopy derived functional traits that were used and modeled with random forests have been found to be clearly expressed in both imaging spectroscopy and multispectral data (Gates et al., 1965; Tucker, 1980; Asner and Vitousek, 2005; Sánchez-Azofeifa et al., 2009; Ustin et al., 2012; Singh et al., 2015), which is supported by the performance of the random forest models.

The expanding reach of imaging spectroscopy airborne campaigns and current and planned satellite-based imaging spectrometers, such as NASA's planned Surface Biology and Geology (SBG) imaging spectrometer (Stavros et al., 2023), will provide increased availability of data and products over time (Cawse-Nicholson et al., 2021). With increased availability of imaging spectroscopy imagery and products, presented methods like these will become more accessible for modeling pre-fire fuels without spatial data gaps.

4.4. Implications of fuel characteristic modeling and mapping

The fuel characteristic maps developed with imaging spectroscopy and lidar remotely sensed data provide a more direct means to compare in situ fuel measures to remote sensing retrievals (Stavros et al., 2018), which could improve fire effects modeling at the landscape scale (Gale et al., 2021). With a broad suite of included uncertainty statistics for both the fuel characteristic models and maps, the relationship of fuels and emissions can be better constrained to improve estimates of fire emissions. The methodology and the maps from this study could be used in fire effects models, like CONSUME, where the mapped estimates of the physical fuel characteristics can be used in place of the static values and classifications of fuels. We plan to explore further how these fuel characteristics can be used with existing models and fuel emissions data to better constrain the relationship between fuels and fire consumption and emissions.

5. Conclusions

The findings of this paper can be summarized as:

- **Continuous mapping of fuel characteristics:** Developed and applied methodology using AVIRIS imaging spectroscopy, lidar, and field data to produce continuous, spatially explicit maps of pre-fire fuel characteristics.
- **Uncertainty and model performance:** Quantified uncertainty and achieved NRMSE values around or below 20 % for most fuel characteristics with strong validation performance.
- **Applicability across different fire types and regimes:** Successfully applied the fuel mapping methodology to a large wildfire and prescribed crown fires that demonstrate potential for broader applications in different fire regimes.

In this study, we evaluated the potential for using imaging spectroscopy and lidar data to model and map continuous fuel characteristics before three Rx crown fires and a wildfire. We also present a method to fill in remote sensing spatial data gaps that result from the limited extent of airborne data collections. The methodology presented produced models that had consistent performance and NRMSE values that were around or under 20 %. When the models were applied to the remote sensing data of the fire locations, the maps had high proportions of high confidence estimates. This methodology is the first to use imaging spectroscopy and lidar data to model, continuously map, and quantify uncertainty of canopy, surface, and ground pre-fire fuel characteristics that can be used for fire consumption and emissions modeling. As imaging spectroscopy and lidar platforms and data become increasingly available, the methods and findings to consistently map pre-fire fuel characteristics presented in this study provide a means to constrain the relationship between fuels and fire emissions.

The need for continuous representations of fuels with quantified uncertainty will help constrain the role and relationship between fuels and fire effects. Specifically, providing an avenue for continuous maps of fuel characteristics would allow for the estimation of error from fuels in fire consumption and emissions estimates. Such quantitative estimation with uncertainty is not possible based on unitless, dNBR-derived severity maps. The methodology in this study provides a way for fuel characteristics to be mapped wherever data is available. We expect these methods to accommodate of a variety of sensor types and be capable of modeling fuel characteristics beyond those presented in this study. Future work should explore the generalizability of the models and extent to which these models can be applied to map fuel characteristics both spatially and temporally. With anticipated spaceborne sensors like the planned Surface Biology and Geology (SBG) imaging spectrometer (Stavros et al., 2023), the methods in this study have potential for global application. Through the SBG imaging spectrometer, it would be possible to quantify pre-fire fuel characteristics across the globe to estimate fire effects, like emissions, for any wildfire event.

CRediT authorship contribution statement

Clare M. Saiki: Writing – original draft, Visualization, Validation, Software, Project administration, Methodology, Investigation, Funding acquisition, Formal analysis, Data curation, Conceptualization. **Dar A. Roberts:** Writing – review & editing, Supervision, Resources, Methodology, Funding acquisition. **E. Natasha Stavros:** Writing – review & editing, Supervision, Project administration, Methodology, Funding acquisition, Conceptualization. **Andrew T. Hudak:** Writing – review & editing, Methodology, Investigation, Funding acquisition, Data curation. **Nancy H.F. French:** Writing – review & editing, Supervision, Methodology. **Olga Kalashnikova:** Writing – review & editing, Supervision, Methodology, Investigation, Conceptualization. **Michael J. Garay:** Writing – review & editing, Supervision, Methodology. **T. Ryan McCarley:** Writing – review & editing, Investigation, Formal analysis, Data curation. **Mark Corrao:** Data curation, Formal analysis, Writing – review & editing.

Declaration of competing interest

The authors declare the following financial interests/personal relationships which may be considered as potential competing interests:

Clare Saiki reports financial support was provided by National Aeronautics and Space Administration Future Investigators in NASA Earth and Space Science and Technology. Clare Saiki reports financial support was provided by USDA Forest Service Rocky Mountain Research Station. Dar Roberts reports financial support was provided by USDA Forest Service Rocky Mountain Research Station. Co-author serves on the Remote Sensing of Environment Editorial Board and previously served as an associated editor - Dar Roberts and Co-author serves on the Remote Sensing of Environment Editorial Board - Andrew Hudak. If there are other authors, they declare that they have no known competing financial interests or personal relationships that could have appeared to influence the work reported in this paper.

Acknowledgements

This research was carried out at the University of California Santa Barbara (UCSB) and through NASA Jet Propulsion Laboratory (JPL) internships. The research was funded by NASA (80NSSC22K1447) and the USDA Forest Service (USFS; 22-CR-11221633-162). This research was supported (in part) by the U.S. Department of Agriculture, Forest Service. Any use of trade, firm, or product names is for descriptive purposes only and does not imply endorsement by the U.S. government. The opinions, findings, and conclusions expressed in this publication are the authors' and do not reflect the views of their institutions. Field data were collected, prepared and provided by USFS through FASMEE and through the joint NASA and NOAA FIREX-AQ campaign. We thank the Confederated Tribes of the Colville Reservation for allowing us to sample fuels on their lands (Research Permit No. 2019-20) and generously sharing the pre-fire lidar data to enable estimation of fuel consumption from the Williams Flats Fire. Airborne Visible/Infrared Imaging Spectrometer data were provided and accessed through the JPL, California Institute of Technology. We thank Carly A. Ringer (Oregon State University) for the detailed study site maps. We thank the

reviewers for their comments and suggestions to improve this manuscript.

Appendix A. Supplementary data

Supplementary data to this article can be found online at https://doi.org/10.1016/j.rse.2025.114721.

Data availability

Data will be made available on request.

References

Adams, J.B., Smith, M.O., Gillespie, A.R., 1993. Imaging spectroscopy: Interpretation based on spectral mixture analysis. In: Englert, C.M., Englert, P.A.J. (Eds.), Remote Geochemical Analysis, Topics in Remote Sensing, Vol. 4. Cambridge University Press, pp. 145–166.

Ahn, S.C., Bae, J., 2022. Forecasting with partial least squares when a large number of predictors are available. SSRN Electron. J. https://doi.org/10.2139/ssrn.4248450.

Alonso-Rego, C., Arellano-Pérez, S., Guerra-Hernández, J., Molina-Valero, J.A., Martínez-Calvo, A., Pérez-Cruzado, C., Castedo-Dorado, F., González-Ferreiro, E., Álvarez-González, J.G., Ruiz-González, A.D., 2021. Estimating stand and fire-related surface and canopy fuel variables in pine stands using low-density airborne and single-scan terrestrial laser scanning data. Remote Sens. 13 (24), Article 24. https://doi.org/10.3390/rs13245170.

Andreu, A.G., Shea, D., Parresol, B.R., Ottmar, R.D., 2012. Evaluating fuel complexes for fire hazard mitigation planning in the southeastern United States. For. Ecol. Manag. 273, 4–16. https://doi.org/10.1016/j.foreco.2011.06.040.

Asner, G.P., Vitousek, P.M., 2005. Remote analysis of biological invasion and biogeochemical change. Proc. Natl. Acad. Sci. 102 (12), 4383–4386. https://doi.org/10.1073/pnas.0500823102.

Asner, G.P., Martin, R.E., Carranza-Jiménez, L., Sinca, F., Tupayachi, R., Anderson, C.B., Martinez, P., 2014. Functional and biological diversity of foliar spectra in tree canopies throughout the Andes to Amazon region. New Phytol. 204 (1), 127–139. https://doi.org/10.1111/nph.12895.

Asner, G.P., Martin, R.E., Anderson, C.B., Knapp, D.E., 2015. Quantifying forest canopy traits: imaging spectroscopy versus field survey. Remote Sens. Environ. 158, 15–27. https://doi.org/10.1016/j.rse.2014.11.011.

Breiman, L., 2001. Random forests. Mach. Learn. 45 (1), 5–32. https://doi.org/10.1023/A:1010933404324.

Bright, B.C., Hudak, A.T., Meddens, A.J.H., Hawbaker, T.J., Briggs, J.S., Kennedy, R.E., 2017. Prediction of Forest canopy and surface fuels from Lidar and satellite time series data in a bark beetle-affected Forest. Forests 8 (9). https://doi.org/10.3390/f8090322 article 9.

Bright, B.C., Hudak, A.T., McCarley, T.R., Spannuth, A., Sánchez-López, N., Ottmar, R.D., Soja, A.J., 2022. Multitemporal lidar captures heterogeneity in fuel loads and consumption on the Kaibab plateau. Fire Ecol. 18 (1), 18. https://doi.org/10.1186/s42408-022-00142-7.

Burke, M., Driscoll, A., Heft-Neal, S., Xue, J., Burney, J., Wara, M., 2021. The changing risk and burden of wildfire in the United States. Proc. Natl. Acad. Sci. 118 (2). https://doi.org/10.1073/pnas.2011048118.

Burnett, A.C., Anderson, J., Davidson, K.J., Ely, K.S., Lamour, J., Li, Q., Morrison, B.D., Yang, D., Rogers, A., Serbin, S.P., 2021. A best-practice guide to predicting plant traits from leaf-level hyperspectral data using partial least squares regression. J. Exp. Bot. 72 (18), 6175–6189. https://doi.org/10.1093/jxb/erab295.

Cawse-Nicholson, K., Townsend, P.A., Schimel, D., Assiri, A.M., Blake, P.L., Buongiorno, M.F., Campbell, P., Carmon, N., Casey, K.A., Correa-Pabón, R.E., Dahlin, K.M., Dashti, H., Dennison, P.E., Dierssen, H., Erickson, A., Fisher, J.B., Frouin, R., Gatebe, C.K., Gholizadeh, H., Zhang, Q., 2021. NASA's surface biology and geology designated observable: a perspective on surface imaging algorithms. Remote Sens. Environ. 257, 112349. https://doi.org/10.1016/j.rse.2021.112349.

Chapin, F.S., III., 2003. Effects of plant traits on ecosystem and regional processes: a conceptual framework for predicting the consequences of global change. Ann. Bot. 91 (4), 455–463. https://doi.org/10.1093/aob/mcg041.

Christian, T.J., Kleiss, B., Yokelson, R.J., Holzinger, R., Crutzen, P.J., Hao, W.M., Saharjo, B.H., Ward, D.E., 2003. Comprehensive laboratory measurements of biomass-burning emissions: 1. Emissions from Indonesian, African, and other fuels. J. Geophys. Res.-Atmos. 108 (D23). https://doi.org/10.1029/2003JD003704.

Chuvieco, E., Salas, J., 1996. Mapping the spatial distribution of forest fire danger using GIS. Int. J. Geogr. Inf. Syst. 10 (3), 333–345. https://doi.org/10.1080/02693799608902082.

Cornwell, W.K., Cornelissen, J.H.C., Amatangelo, K., Dorrepaal, E., Eviner, V.T., Godoy, O., Hobbie, S.E., Hoorens, B., Kurokawa, H., Pérez-Harguindeguy, N., Quested, H.M., Santiago, L.S., Wardle, D.A., Wright, I.J., Aerts, R., Allison, S.D., Van Bodegom, P., Brovkin, V., Chatain, A., Westoby, M., 2008. Plant species traits are the predominant control on litter decomposition rates within biomes worldwide. Ecol. Lett. 11 (10), 1065–1071. https://doi.org/10.1111/j.1461-0248.2008.01219.x.

Curran, P.J., 1989. Remote sensing of foliar chemistry. Remote Sens. Environ. 30 (3), 271–278. https://doi.org/10.1016/0034-4257(89)90069-2.

Curran, P.J., Dungan, J.L., Macler, B.A., Plummer, S.E., Peterson, D.L., 1992. Reflectance spectroscopy of fresh whole leaves for the estimation of chemical concentration. Remote Sens. Environ. 39 (2), 153–166. https://doi.org/10.1016/0034-4257(92)90133-5.

Curran, P.J., Dungan, J.L., Peterson, D.L., 2001. Estimating the foliar biochemical concentration of leaves with reflectance spectrometry: testing the Kokaly and Clark methodologies. Remote Sens. Environ. 76 (3), 349–359. https://doi.org/10.1016/S0034-4257(01)00182-1.

de Groot, W., 2012. CANFIRE model. Natural Resources Canada. Canadian Forest Service. Great Lakes forestry Centre. Sault Ste. Marie, Ontario. Frontline Express 62, 2p.

Dennison, P.E., Roberts, D.A., 2003. Endmember selection for multiple endmember spectral mixture analysis using endmember average RMSE. Remote Sens. Environ. 87 (2), 123–135. https://doi.org/10.1016/S0034-4257(03)00135-4.

Dennison, P.E., Halligan, K.Q., Roberts, D.A., 2004. A comparison of error metrics and constraints for multiple endmember spectral mixture analysis and spectral angle mapper. Remote Sens. Environ. 93 (3), 359–367. https://doi.org/10.1016/j.rse.2004.07.013.

Dennison, P.E., Brewer, S.C., Arnold, J.D., Moritz, M.A., 2014. Large wildfire trends in the western United States, 1984–2011. Geophys. Res. Lett. 41 (8), 2928–2933. https://doi.org/10.1002/2014GL059576.

Domingo, D., de la Riva, J., Lamelas, M.T., García-Martín, A., Ibarra, P., Echeverría, M., Hoffrén, R., 2020. Fuel type classification using airborne laser scanning and sentinel 2 data in Mediterranean Forest affected by wildfires. Remote Sens. 12(21), Article 21. https://doi.org/10.3390/rs12213660.

Eagle, P.C., Cronan, J.B., McCarley, T.R., Bright, B.C., Hudak, A.T., 2024. Field Plot Measurements from the 2017–2020 FASMEE Rx Fires. Forest Service Research Data Archive, Fort Collins, CO. https://doi.org/10.2737/RDS-2024-0049. Updated 04 November 2024.

Evans, J.R., 1989. Photosynthesis and nitrogen relationships in leaves of C3 plants. Oecologia 78 (1), 9–19. https://doi.org/10.1007/BF00377192.

Evans, J.S., Murphy, A.M., 2019. rfUtilities. R package version 2, 13. https://cran.r-project.org/package=rfUtilities.

Falkowski, M.J., Smith, A.M.S., Hudak, A.T., Gessler, P.E., Vierling, L.A., Crookston, N.L., 2006. Automated estimation of individual conifer tree height and crown diameter via two-dimensional spatial wavelet analysis of lidar data. Can. J. Remote. Sens. 32 (2), 153–161. https://doi.org/10.5589/m06-005.

Falkowski, M.J., Evans, J.S., Martinuzzi, S., Gessler, P.E., Hudak, A.T., 2009. Characterizing forest succession with lidar data: an evaluation for the inland northwest, USA. Remote Sens. Environ. 113 (5), 946–956. https://doi.org/10.1016/j.rse.2009.01.003.

Flannigan, M.D., Krawchuk, M.A., de Groot, W.J., Wotton, B.M., Gowman, L.M., 2009. Implications of changing climate for global wildland fire. Int. J. Wildland Fire 18 (5), 483–507. https://doi.org/10.1071/WF08187.

Fortin, M., 2021. Comparison of uncertainty quantification techniques for national greenhouse gas inventories. Mitig. Adapt. Strateg. Glob. Chang. 26 (2), 1–20.

Fourty, Th., Baret, F., Jacquemoud, S., Schmuck, G., Verdebout, J., 1996. Leaf optical properties with explicit description of its biochemical composition: direct and inverse problems. Remote Sens. Environ. 56 (2), 104–117. https://doi.org/10.1016/0034-4257(95)00234-0.

French, N.H.F., Goovaerts, P., Kasischke, E.S., 2004. Uncertainty in estimating carbon emissions from boreal forest fires. J. Geophys. Res. Atmos. 109 (D14). https://doi.org/10.1029/2003JD003635.

Gale, M.G., Cary, G.J., Van Dijk, A.I.J.M., Yebra, M., 2021. Forest fire fuel through the lens of remote sensing: review of approaches, challenges and future directions in the remote sensing of biotic determinants of fire behaviour. Remote Sens. Environ. 255, 112282. https://doi.org/10.1016/j.rse.2020.112282.

García, M., Saatchi, S., Casas, A., Koltunov, A., Ustin, S.L., Ramirez, C., Balzter, H., 2017. Extrapolating Forest canopy fuel properties in the California rim fire by combining airborne LiDAR and Landsat OLI data. Remote Sens. 9 (4), Article 4. https://doi.org/10.3390/rs9040394.

Garthwaite, P.H., 1994. An interpretation of partial least squares. J. Am. Stat. Assoc. 89 (425), 122–127. https://doi.org/10.2307/2291207.

Gates, D.M., Keegan, H.J., Schleter, J.C., Weidner, V.R., 1965. Spectral properties of plants. Appl. Opt. 4 (1), 11–20. https://doi.org/10.1364/AO.4.000011.

Green, R.O., Eastwood, M.L., Sarture, C.M., Chrien, T.G., Aronsson, M., Chippendale, B. J., Faust, J.A., Pavri, B.E., Chovit, C.J., Solis, M., Olah, M.R., Williams, O., 1998. Imaging spectroscopy and the airborne visible/infrared imaging spectrometer (AVIRIS). Remote Sens. Environ. 65 (3), 227–248. https://doi.org/10.1016/S0034-4257(98)00064-9.

Hijmans, R., 2023a. Raster: geographic data analysis and modeling. R package version 3, 6–26. https://CRAN.R-project.org/package=raster.

Hijmans, R., 2023b. Terra: spatial data analysis. R package version 1, 7–65. https://CRAN.R-project.org/package=terra.

Höskuldsson, A., 1988. PLS regression methods. J. Chemom. 2 (3), 211–228. https://doi.org/10.1002/cem.1180020306.

Hudak, A.T., Kato, A., Bright, B.C., Loudermilk, E.L., Hawley, C., Restaino, J.C., Ottmar, R.D., Prata, G.A., Cabo, C., Prichard, S.J., Rowell, E.M., Weise, D.R., 2020. Towards spatially explicit quantification of pre- and postfire fuels and fuel consumption from traditional and point cloud measurements. For. Sci. https://doi.org/10.1093/Forsci/Fxz085.

Hudak, A.T., McCarley, T.R., Bright, B.C., n.d. In review. Field Observations of Trees, Shrubs and Fuels Measured for the Fire and Smoke Model Evaluation Experiment (FASMEE), Western Wildfires Campaign. Service Research Data Archive, Fort Collins, CO: Forest.

Jakubowksi, M.K., Guo, Q., Collins, B., Stephens, S., Kelly, M., 2013. Predicting surface fuel models and fuel metrics using Lidar and CIR imagery in a dense, mountainous Forest. Photogramm. Eng. Remote. Sens. 79 (1), 37–49. https://doi.org/10.14358/PERS.79.1.37.

Kazakou, E., Vile, D., Shipley, B., Gallet, C., Garnier, E., 2006. Co-variations in litter decomposition, leaf traits and plant growth in species from a Mediterranean old-field succession. Funct. Ecol. 20 (1), 21–30. https://doi.org/10.1111/j.1365-2435.2006.01080.x.

Keane, R.E., 2015. Wildland fuel fundamentals and applications. Springer International Publishing. https://doi.org/10.1007/978-3-319-09015-3.

Keane, R.E., Burgan, R., van Wagtendonk, J., 2001. Mapping wildland fuels for fire management across multiple scales: integrating remote sensing, GIS, and biophysical modeling. Int. J. Wildland Fire 10 (4), 301–319. https://doi.org/10.1071/wf01028.

Kennedy, M.C., Prichard, S.J., McKenzie, D., French, N.H.F., 2020. Quantifying how sources of uncertainty in combustible biomass propagate to prediction of wildland fire emissions. Int. J. Wildland Fire 29 (9), 793. https://doi.org/10.1071/WF19160.

Key, C.H., Benson, N.C., 2006. Landscape assessment (LA). In: Lutes, Duncan, C., Keane, Robert E., Caratti, John F., Key, Carl H., Benson, Nathan C., Sutherland, Steve, Gangi, Larry J. (Eds.), *FIREMON: fire effects monitoring and inventory system. Gen. Tech. Rep. RMRS-GTR-164-CD. Fort Collins, CO: U.S. Department of Agriculture, Forest Service, Rocky Mountain Research Station. p. LA-1-55*, *164*. https://www.fs.usda.gov/treesearch/pubs/24066.

Keye, J.K., Varner, J.M., Dugaw, C.J., 2014. Spatial and temporal variability of forest floor duff characteristics in long-unburned Pinus palustris forests. Can. J. For. Res. 44 (12), 1477–1486. https://doi.org/10.1139/cjfr-2014-0223.

Labenski, P., Ewald, M., Schmidtlein, S., Heinsch, F.A., Fassnacht, F.E., 2023. Quantifying surface fuels for fire modelling in temperate forests using airborne lidar and Sentinel-2: potential and limitations. Remote Sens. Environ. 295, 113711. https://doi.org/10.1016/j.rse.2023.113711.

Larkin, N.K., O'Neill, S.M., Solomon, R., Raffuse, S., Strand, T., Sullivan, D.C., Krull, C., Rorig, M., Peterson, J., Ferguson, S.A., 2010. The BlueSky smoke modeling framework. Int. J. Wildland Fire 18 (8), 906–920. https://doi.org/10.1071/WF07086.

Larkin, N., Strand, T., Drury, S., Raffuse, S., Solomon, R., O'Neill, S., Wheeler, N., Huang, S., Roring, M., Hafner, H.. Phase 1 of the smoke and emissions model intercomparison project (SEMIP): creation of SEMIP and evaluation of current models. JFSP research project reports. https://digitalcommons.unl.edu/jfspresearch/42.

Lasaponara, R., Lanorte, A., Pignatti, S., 2006. Characterization and mapping of fuel types for the Mediterranean ecosystems of Pollino National Park in southern Italy by using hyperspectral MIVIS data. Earth Interact. 10 (13), 1–11. https://doi.org/10.1175/EI165.1.

Liaw, A., Wiener, M., 2002. Classification and regression by randomForest. R News 2 (3), 18–22.

Littell, J.S., Oneil, E.E., McKenzie, D., Hicke, J.A., Lutz, J.A., Norheim, R.A., Elsner, M. M., 2010. Forest ecosystems, disturbance, and climatic change in Washington state, USA. Clim. Chang. 102 (1–2), 129–158. https://doi.org/10.1007/s10584-010-9858-x.

Liu, Y.L., Goodrick, S.A., Stanturf, J., 2013. Future U.S. wildfire potential trends projected using a dynamically downscaled climate change scenario. For. Ecol. Manag. 294, 120–135. https://doi.org/10.1016/j.foreco.2012.06.049.

Marino, E., Ranz, P., Tomé, J.L., Noriega, M.Á., Esteban, J., Madrigal, J., 2016. Generation of high-resolution fuel model maps from discrete airborne laser scanner and Landsat-8 OLI: a low-cost and highly updated methodology for large areas. Remote Sens. Environ. 187, 267–280. https://doi.org/10.1016/j.rse.2016.10.020.

Martin, M.E., Plourde, L.C., Ollinger, S.V., Smith, M.-L., McNeil, B.E., 2008. A generalizable method for remote sensing of canopy nitrogen across a wide range of forest ecosystems. Remote Sens. Environ. 112 (9), 3511–3519. https://doi.org/10.1016/j.rse.2008.04.008.

Mauro, F., Hudak, A.T., Fekety, P.A., Frank, B., Temesgen, H., Bell, D.M., Gregory, M.J., McCarley, T.R., 2021. Regional modeling of Forest fuels and structural attributes using airborne laser scanning data in Oregon. Remote Sens. 13 (2). https://doi.org/10.3390/rs13020261. Article 2.

McCarley, T.R., Hudak, A.T., Restaino, J.C., Billmire, M., French, N.H.F., Ottmar, R.D., Hass, B., Zarzana, K., Goulden, T., Volkamer, R., 2022. A Comparison of Multitemporal Airborne Laser Scanning Data and the Fuel Characteristics Classification System for Estimating Fuel Load and Consumption. Journal of Geophysical Research: Biogeosciences 127 (5), e2021JG006733. https://doi.org/10.1029/2021JG006733.

McCarley, T.R., Hudak, A.T., Sparks, A.M., Vaillant, N.M., Meddens, A.J.H., Trader, L., Mauro, F., Kreitler, J., Boschetti, L., 2020. Estimating wildfire fuel consumption with multitemporal airborne laser scanning data and demonstrating linkage with MODIS-derived fire radiative energy. Remote Sens. Environ. 251, 112114. https://doi.org/10.1016/j.rse.2020.112114.

McCarley, T.R., Hudak, A.T., Bright, B.C., Cronan, J., Eagle, P., Ottmar, R., Watts, A.C., 2024. Generating fuel consumption maps on prescribed fire experiments from airborne laser scanning. Int. J. Wildland Fire 33, WR23160. https://doi.org/10.1071/WF23160.

McKenzie, D., Gedalof, Z., Peterson, D.L., Mote, P., 2004. Climatic change, wildfire, and conservation. Conserv. Biol. 18 (4), 890–902. https://doi.org/10.1111/j.1523-1739.2004.00492.x.

McKenzie, D., Shankar, U., Keane, R.E., Stavros, E.N., Heilman, W.E., Fox, D.G., Riebau, A.C., 2014. Smoke consequences of new wildfire regimes driven by climate change. Earth's Future 2 (2), 35–59. https://doi.org/10.1002/2013EF000180.

Miyanishi, K., 2001. Chapter 13—Duff consumption. In: Johnson, E.A., Miyanishi, K. (Eds.), Forest Fires. Academic Press, pp. 437–475. https://doi.org/10.1016/B978-012386660-8/50015-5.

Moreno-Martínez, Á., Camps-Valls, G., Kattge, J., Robinson, N., Reichstein, M., van Bodegom, P., Kramer, K., Cornelissen, J.H.C., Reich, P., Bahn, M., Niinemets, Ü., Peñuelas, J., Craine, J.M., Cerabolini, B.E.L., Minden, V., Laughlin, D.C., Sack, L., Allred, B., Baraloto, C., Running, S.W., 2018. A methodology to derive global maps of leaf traits using remote sensing and climate data. Remote Sens. Environ. 218, 69–88. https://doi.org/10.1016/j.rse.2018.09.006.

Mutlu, M., Popescu, S.C., Stripling, C., Spencer, T., 2008. Mapping surface fuel models using lidar and multispectral data fusion for fire behavior. Remote Sens. Environ. 112 (1), 274–285. https://doi.org/10.1016/j.rse.2007.05.005.

National Academies of Sciences, Engineering, and Medicine, 2018. Thriving on our changing planet: a decadal strategy for earth observation from space. The National Academies Press. https://doi.org/10.17226/24938.

Ottmar, R.D., 2014. Wildland fire emissions, carbon, and climate: modeling fuel consumption. For. Ecol. Manag. 317, 41–50, 41–50. https://doi.org/10.1016/j.foreco.2013.06.010.

Ottmar, R.D., Sandberg, D.V., Riccardi, C.L., Prichard, S.J., 2007. An overview of the fuel characteristic classification system—quantifying, classifying, and creating fuelbeds for resource planning. Can. J. For. Res. 37 (12), 2383–2393. https://doi.org/10.1139/X07-077.

Parresol, B.R., Blake, J.I., Thompson, A.J., 2012. Effects of overstory composition and prescribed fire on fuel loading across a heterogeneous managed landscape in the southeastern USA. For. Ecol. Manag. 273, 29–42. https://doi.org/10.1016/j.foreco.2011.08.003.

Peterson, J.L., 1987. Analysis and Reduction of the Errors of Predicting Prescribed Burn Emissions. University of Washington, Seattle, WA, p. 70 (M.S. thesis.).

Pierce, A.D., Farris, C.A., Taylor, A.H., 2012. Use of random forests for modeling and mapping forest canopy fuels for fire behavior analysis in Lassen volcanic National Park, California, USA. For. Ecol. Manag. 279, 77–89. https://doi.org/10.1016/j.foreco.2012.05.010.

Price, O.F., Gordon, C.E., 2016. The potential for LiDAR technology to map fire fuel hazard over large areas of Australian forest. J. Environ. Manag. 181, 663–673. https://doi.org/10.1016/j.jenvman.2016.08.042.

Prichard, S.J., 2007. Consume user's Guide. Pacific Wildland Fire Sciences Laboratory USDA Forest Service. (Seattle, WA) Available at http:// www.fs.fed.us/pnw/fera/research/smoke/consume/consume30_users_ guide.pdf.

Prichard, S.J., Kennedy, M.C., Andreu, A.G., Eagle, P.C., French, N.H., Billmire, M., 2019. Next-generation biomass mapping for regional emissions and carbon inventories: incorporating uncertainty in wildland fuel characterization. J. Geophys. Res. Biogeosci. 124 (12), 3699–3716. https://doi.org/10.1029/2019JG005083.

Quested, H., Eriksson, O., Fortunel, C., Garnier, E., 2007. Plant traits relate to whole-community litter quality and decomposition following land use change. Funct. Ecol. 21 (6), 1016–1026. https://doi.org/10.1111/j.1365-2435.2007.01324.x.

R Core Team, 2023. R: A Language and Environment for Statistical Computing. R Foundation for Statistical Computing, Vienna, Austria. https://www.R-project.org/.

Randerson, J.T., van der Werf, G.R., Giglio, L., Collatz, G.J., Kasibhatla, P.S., 2018. Global Fire Emissions Database, Version 4.1 (GFEDv4). ORNL DAAC, Oak Ridge, Tennessee, USA. https://doi.org/10.3334/ORNLDAAC/1293.

Reich, P.B., Walters, M.B., Ellsworth, D.S., 1997. From tropics to tundra: global convergence in plant functioning. Proc. Natl. Acad. Sci. 94 (25), 13730–13734. https://doi.org/10.1073/pnas.94.25.13730.

Roberts, D.W., Cooper, S.V., 1989. Concepts and techniques of vegetation mapping. In: Ferguson, D., Morgan, P., Johnson, F.D. (Eds.), Land Classifications Based on Vegetation: Applications for Resource Management. USDA For. Serv. Gen, Ogden, UT, pp. 90–96. Tech. Rep. INT-257,.

Roberts, D.A., Smith, M.O., Adams, J.B., 1993. Green vegetation, nonphotosynthetic vegetation, and soils in AVIRIS data. Remote Sens. Environ. 44 (2), 255–269. https://doi.org/10.1016/0034-4257(93)90020-X.

Roberts, D.A., Gardner, M., Church, R., Ustin, S., Scheer, G., Green, R.O., 1998. Mapping chaparral in the Santa Monica Mountains using multiple endmember spectral mixture models. Remote Sens. Environ. 65 (3), 267–279. https://doi.org/10.1016/S0034-4257(98)00037-6.

Roberts, D.A., Dennison, P.E., Gardner, M.E., Hetzel, Y., Ustin, S.L., Lee, C.T., 2003. Evaluation of the potential of Hyperion for fire danger assessment by comparison to the airborne visible/infrared imaging spectrometer. IEEE Trans. Geosci. Remote Sens. 41 (6), 1297–1310. https://doi.org/10.1109/TGRS.2003.812904.

Roberts, D.A., Ustin, S.L., Ogunjemiyo, S., Greenberg, J., Dobrowski, S.Z., Chen, J., Hinckley, T.M., 2004. Spectral and structural measures of northwest Forest vegetation at leaf to landscape scales. Ecosystems 7 (5), 545–562. https://doi.org/10.1007/s10021-004-0144-5.

Roberts, D.A., Dennison, P.E., Peterson, S., Sweeney, S., Rechel, J., 2006. Evaluation of airborne visible/infrared imaging spectrometer (AVIRIS) and moderate resolution imaging spectrometer (MODIS) measures of live fuel moisture and fuel condition in a shrubland ecosystem in southern California: AVIRIS AND MODIS LIVE FUEL MOISTURE. J. Geophys. Res. Biogeosci. 111 (G4). https://doi.org/10.1029/2005JG000113.

Roberts, D.A., Halligan, K., Dennison, P., Dudley, K., Somers, B., Crabbe, A., 2019. Viper tools 2.1, self published user manual, 92 pp. https://drive.google.com/drive/u/1/folders/14URF-Xi38ri7yWQFDjlKxXgkcaYCu9d0.

Rollins, M.G., 2009. LANDFIRE: a nationally consistent vegetation, wildland fire, and fuel assessment. Int. J. Wildland Fire 18 (3), 235. https://doi.org/10.1071/WF08088.

Roussel, J.R., Auty, D., Coops, N.C., Tompalski, P., Goodbody, T.R.H., Sánchez Meador, A., Bourdon, J.F., De Boissieu, F., Achim, A., 2020. lidR : an R package for

analysis of airborne laser scanning (ALS) data. In: Remote sensing of environment, p. 112061. https://doi.org/10.1016/j.rse.2020.112061, 251 (august).
Ryan, K.C., Opperman, T.S., 2013. LANDFIRE - a national vegetation/fuels data base for use in fuels treatment, restoration, and suppression planning. For. Ecol. Manag. 294 (208–216), 208–216. https://doi.org/10.1016/j.foreco.2012.11.003.
Sánchez-Azofeifa, G.A., Castro, K., Wright, S.J., Gamon, J., Kalacska, M., Rivard, B., Schnitzer, S.A., Feng, J.L., 2009. Differences in leaf traits, leaf internal structure, and spectral reflectance between two communities of lianas and trees: implications for remote sensing in tropical environments. Remote Sens. Environ. 113 (10), 2076–2088. https://doi.org/10.1016/j.rse.2009.05.013.
Santiago, L.S., 2007. Extending the leaf economics Spectrum to decomposition: evidence from a tropical Forest. Ecology 88 (5), 1126–1131. https://doi.org/10.1890/06-1841.
Seiler, W., Crutzen, P.J., 1980. Estimates of gross and net fluxes of carbon between the biosphere and the atmosphere from biomass burning. Clim. Chang. 2 (3), 207–247. https://doi.org/10.1007/BF00137988.
Serbin, S.P., Singh, A., McNeil, B.E., Kingdon, C.C., Townsend, P.A., 2014. Spectroscopic determination of leaf morphological and biochemical traits for northern temperate and boreal tree species. Ecol. Appl. 24 (7), 1651–1669.
Serrano, L., Ustin, S.L., Roberts, D.A., Gamon, J.A., Peñuelas, J., 2000. Deriving water content of chaparral vegetation from AVIRIS data. Remote Sens. Environ. 74 (3), 570–581. https://doi.org/10.1016/S0034-4257(00)00147-4.
Singh, A., Serbin, S.P., McNeil, B.E., Kingdon, C.C., Townsend, P.A., 2015. Imaging spectroscopy algorithms for mapping canopy foliar chemical and morphological traits and their uncertainties. Ecol. Appl. 25 (8), 2180–2197. https://doi.org/10.1890/14-2098.1.
Stavros, E.N., Abatzoglou, J.T., McKenzie, D., Larkin, N.K., 2014. Regional projections of the likelihood of very large wildland fires under a changing climate in the contiguous Western United States. Clim. Chang. 126 (3), 455–468. https://doi.org/10.1007/s10584-014-1229-6.
Stavros, E.N., Coen, J., Peterson, B., Singh, H., Kennedy, K., Ramirez, C., Schimel, D., 2018. Use of imaging spectroscopy and LIDAR to characterize fuels for fire behavior prediction. Remote Sens. Appl.: Soc. Environ. 11, 41–50. https://doi.org/10.1016/j.rsase.2018.04.010.
Stavros, E.N., Chrone, J., Cawse-Nicholson, K., Freeman, A., Glenn, N.F., Guild, L., Kokaly, R., Lee, C., Luvall, J., Pavlick, R., Poulter, B., Schollaert Uz, S., Serbin, S., Thompson, D.R., Townsend, P.A., Turpie, K., Yuen, K., Thome, K., Wang, W., Schimel, D., 2023. Designing an observing system to study the surface biology and geology (SBG) of the earth in the 2020s. J. Geophys. Res. Biogeosci. 128 (1). https://doi.org/10.1029/2021JG006471 e2021JG006471.
Stefanidou, A., Gitas, I.Z., Korhonen, L., Stavrakoudis, D., Georgopoulos, N., 2020. LiDAR-based estimates of Canopy Base height for a dense uneven-aged structured Forest. Remote Sens. 12(10), Article 10. https://doi.org/10.3390/rs12101565.
Stephens, S.L., Agee, J.K., Fulé, P.Z., North, M.P., Romme, W.H., Swetnam, T.W., Turner, M.G., 2013. Managing forests and fire in changing climates. Science 342 (6154), 41–42. https://doi.org/10.1126/science.1240294.
Tane, Z., Roberts, D., Veraverbeke, S., Casas, Á., Ramirez, C., Ustin, S., 2018. Evaluating endmember and band selection techniques for multiple endmember spectral mixture analysis using post-fire imaging spectroscopy. Remote Sens. 10(3), Article 3. https://doi.org/10.3390/rs10030389.
Tucker, C.J., 1980. Remote sensing of leaf water content in the near infrared. Remote Sens. Environ. 10 (1), 23–32. https://doi.org/10.1016/0034-4257(80)90096-6.
Urbanski, S.P., Hao, W.M., Nordgren, B., 2011. The wildland fire emission inventory: Western United States emission estimates and an evaluation of uncertainty. Atmos. Chem. Phys. 11 (24), 12973–13000. https://doi.org/10.5194/acp-11-12973-2011.
US EPA, 2019, August 13. *Health Effects Attributed to Wildfire Smoke* [Overviews and Factsheets]. https://www.epa.gov/wildfire-smoke-course/health-effects-attributed-wildfire-smoke.
US EPA, 2020, October 28. *Research on Health Effects from Air Pollution* [Overviews and Factsheets]. https://www.epa.gov/air-research/research-health-effects-air-pollution.
Ustin, S.L., Riaño, D., Hunt, E.R., 2012. Estimating canopy water content from spectroscopy. Israel J. Plant Sci. 60 (1–2), 9–23. https://doi.org/10.1560/IJPS.60.1-2.9.
Veraverbeke, S., Dennison, P., Gitas, I., Hulley, G., Kalashnikova, O., Katagis, T., Kuai, L., Meng, R., Roberts, D., Stavros, N., 2018. Hyperspectral remote sensing of fire: state-of-the-art and future perspectives. Remote Sens. Environ. 216, 105–121. https://doi.org/10.1016/j.rse.2018.06.020.
Verrelst, J., Rivera, J.P., Gitelson, A., Delegido, J., Moreno, J., Camps-Valls, G., 2016. Spectral band selection for vegetation properties retrieval using Gaussian processes regression. Int. J. Appl. Earth Obs. Geoinf. 52, 554–567. https://doi.org/10.1016/j.jag.2016.07.016.
Wang, Z., Townsend, P.A., Schweiger, A.K., Couture, J.J., Singh, A., Hobbie, S.E., Cavender-Bares, J., 2019. Mapping foliar functional traits and their uncertainties across three years in a grassland experiment. Remote Sens. Environ. 221, 405–416. https://doi.org/10.1016/j.rse.2018.11.016.
Wang, Z., Chlus, A., Geygan, R., Ye, Z., Zheng, T., Singh, A., Couture, J.J., Cavender-Bares, J., Kruger, E.L., Townsend, P.A., 2020. Foliar functional traits from imaging spectroscopy across biomes in eastern North America. New Phytol. 228 (2), 494–511. https://doi.org/10.1111/nph.16711.
Wegesser, T.C., Pinkerton, K.E., Last, J.A., 2009. California wildfires of 2008: coarse and fine particulate matter toxicity. Environ. Health Perspect. 117 (6), 893–897. https://doi.org/10.1289/ehp.0800166.
Wold, S., Sjöström, M., Eriksson, L., 2001. PLS-regression: a basic tool of chemometrics. Chemom. Intell. Lab. Syst. 58 (2), 109–130. https://doi.org/10.1016/S0169-7439(01)00155-1.
Woods, M., Lim, K., Treitz, P., 2008. Predicting forest stand variables from LiDAR data in the Great Lakes - St. Lawrence forest of Ontario. For. Chron. 84 (6), 827–839. https://doi.org/10.5558/tfc84827-6.
Wright, I.J., Reich, P.B., Westoby, M., Ackerly, D.D., Baruch, Z., Bongers, F., Cavender-Bares, J., Chapin, T., Cornelissen, J.H.C., Diemer, M., Flexas, J., Garnier, E., Groom, P.K., Gulias, J., Hikosaka, K., Lamont, B.B., Lee, T., Lee, W., Lusk, C., Villar, R., 2004. The worldwide leaf economics spectrum. Nature 428 (6985), 821–827. https://doi.org/10.1038/nature02403.
Wulder, M.A., White, J.C., Nelson, R.F., Næsset, E., Ørka, H.O., Coops, N.C., Hilker, T., Bater, C.W., Gobakken, T., 2012. Lidar sampling for large-area forest characterization: a review. Remote Sens. Environ. 121, 196–209. https://doi.org/10.1016/j.rse.2012.02.001.